Песчаные интрузии

А.М. Никишин

Северное море

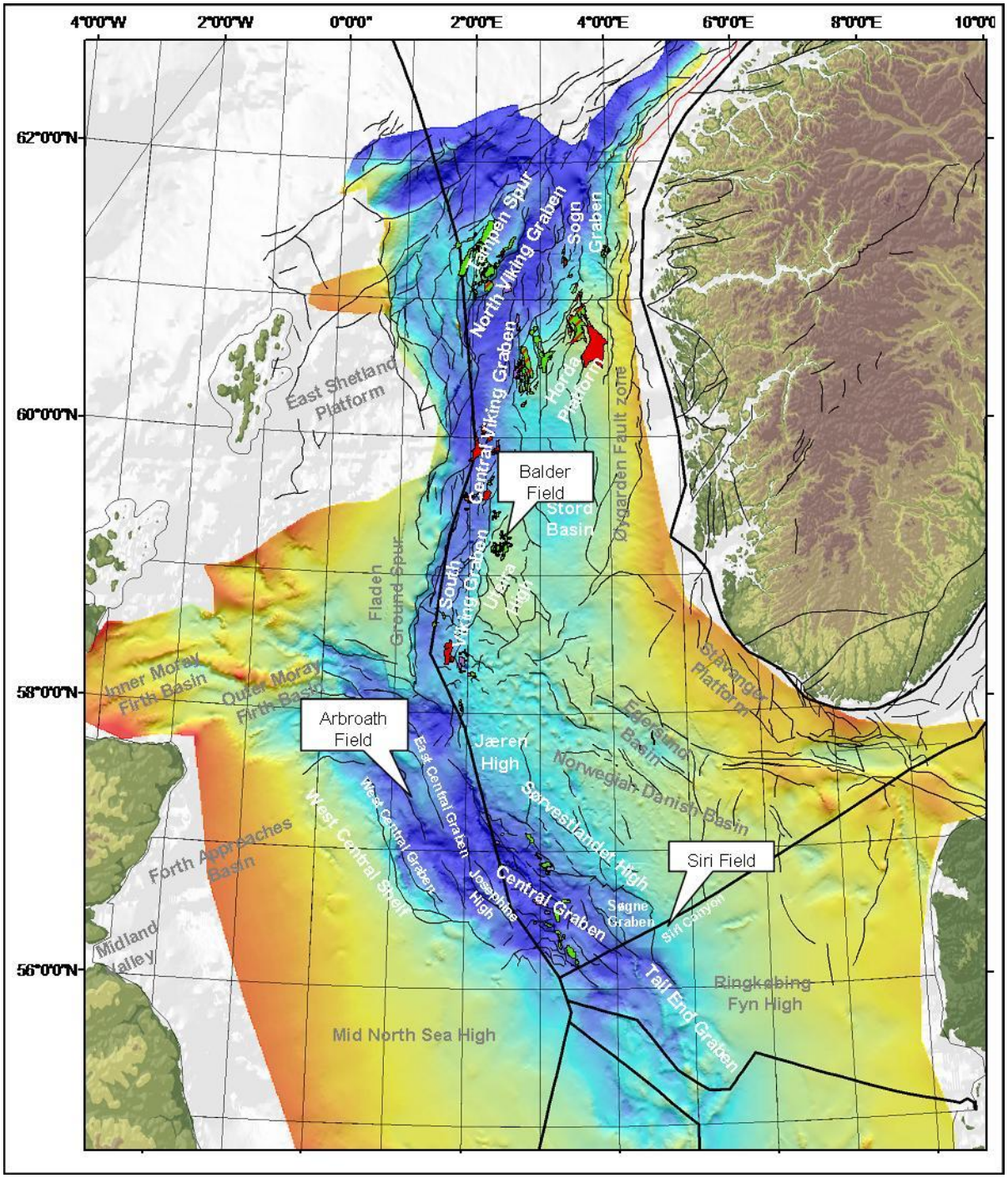

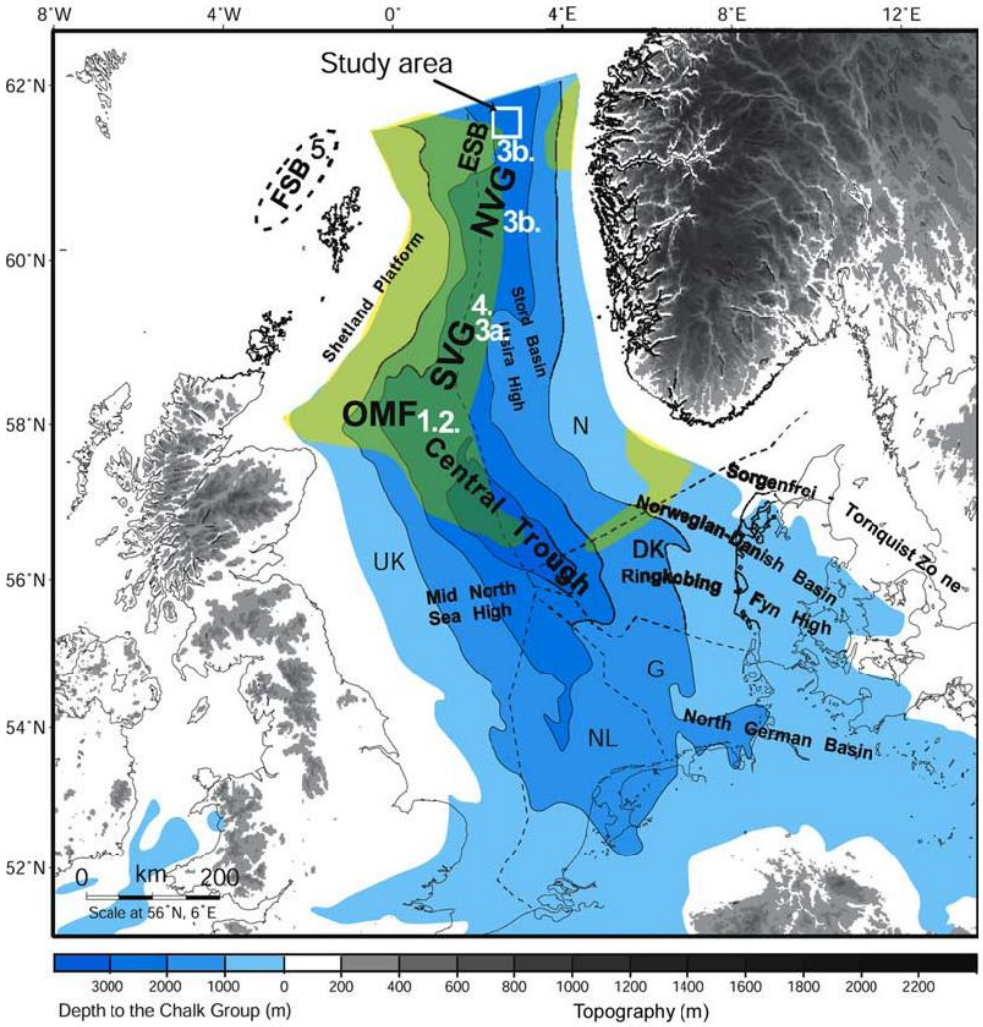

Fig. 1. Depth to the base of the Cenozoic (excl. Danian) and location of major Mesozoic structural elements in the North Sea Basin. Approximate extent of Paleocene sand deposition is indicated by yellow outline. Discordant amplitude anomalies in the Eocene section have been documented from the areas indicated by numbers 1–5. They are registered as follows: 1. Conical sandstone intrusions in the Eocene of the Outer Moray Firth (OMF: Molyneux, 2001; Molyneux et al., 2002); 2. Conical sandstone intrusions in the Eocene of the Outer Moray Firth (Gras & Cartwright, 2002); 3a. V-shaped sandstone intrusions in the South Viking Graben (SVG: Løseth et al., 2003); 3b. V-shaped tuff intrusions, cemented fault planes and/or seismic artefacts in the Eocene of the North Viking Graben (NVG)/Tampen Spur area (Løseth et al., 2003); 4. Conical sandstone intrusions in the Lower-Middle Eocene of the South Viking Graben (Huuse et al., 2004); 5. V-shaped amplitude anomalies in the Paleogene of the Faeroe-Shetland Basin (FSB: Huuse et al., 2001). This study focuses on the northern part of the Tampen Spur area indicated by a rectangle to the east of the East Shetland Basin (ESB).

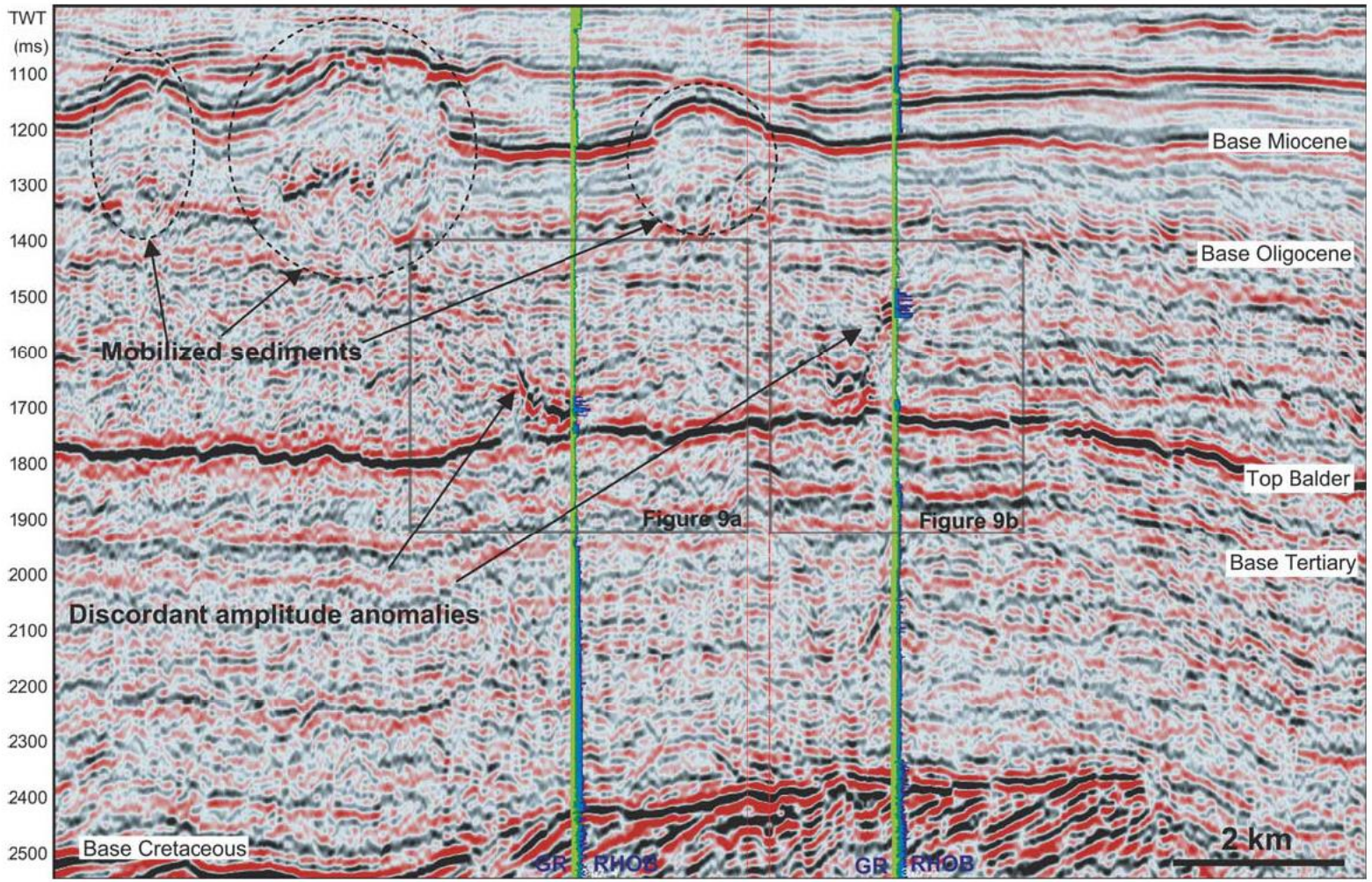

Fig. 3. Conical amplitude anomalies occur within the Eocene of the Tampen Spur area, both above and adjacent to anticlines developed over the crests of tilted Jurassic fault blocks. In the southwestern part of the study area they occur below a zone of extensive mud remobilisation, but show no systematic relation to the intensity of the remobilisation. In some studies the anomalies have been linked to gas chimneys, but there is no consistent relation between the anomalies and chimneys in the underlying section in this study area.

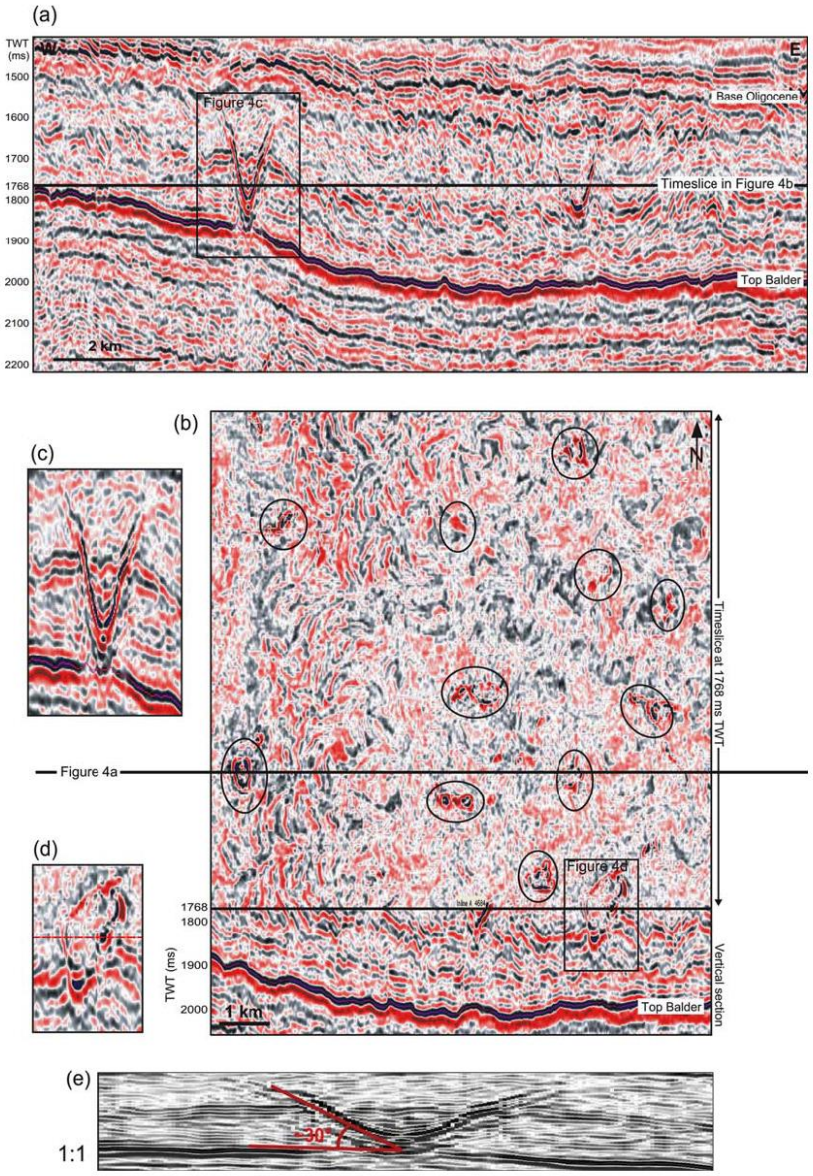

Fig. 4. Conical amplitude anomalies in Norwegian Block 34/5 seen as V-shaped anomalies in cross sections and as near-circular to oval amplitude anomalies in timeslice (1768 ms TWT). The anomalies occur at two levels: one with apexes immediately above Top Balder and one with apexes about 120–150 m above Top Balder (Fig. 8). Anomalies from both levels extend up to 200–300 m above Top Balder. Note that vertical sections are compressed to about 10 × vertical exaggeration. The lowermost panel (e) shows the anomaly from panel (c) at a scale approximately 1:1, showing the true dip of the discordant anomalies that are typically inclined of the order of 30° to the Top Balder surface.

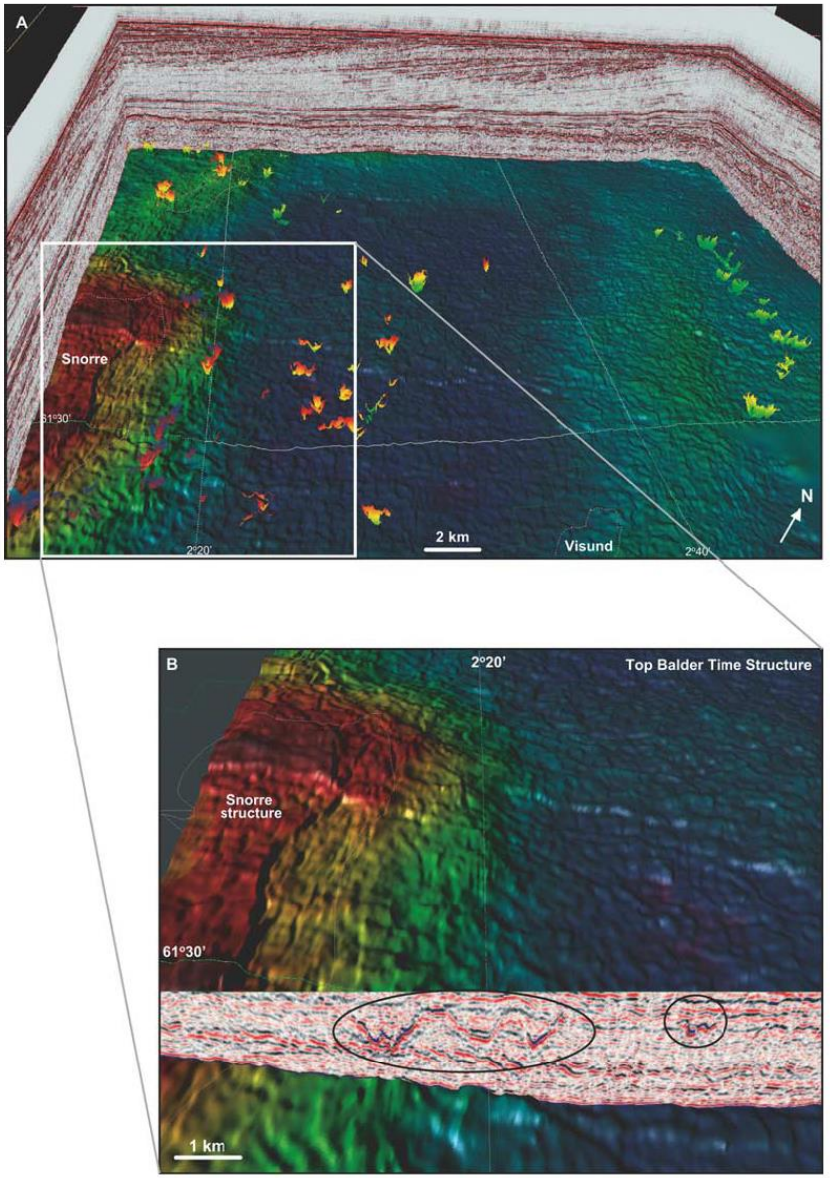

Fig. 6. Top Balder TWT-structure map showing topography formed by drape and differential compaction across the tilted Jurassic fault blocks of the Tampe Spur (crests indicated by red-green colours). The Top Balder represents the top of the Paleocene and any major sandbodies are thus likely to be located belo the surface. Interpreted conical amplitude anomalies are shown as individual surfaces on the regional view (A) and as V-shaped anomalies on a cross section i the close up (B). Note that the anomalies mainly occur along the edges of the anticlinal structures at Top Balder.

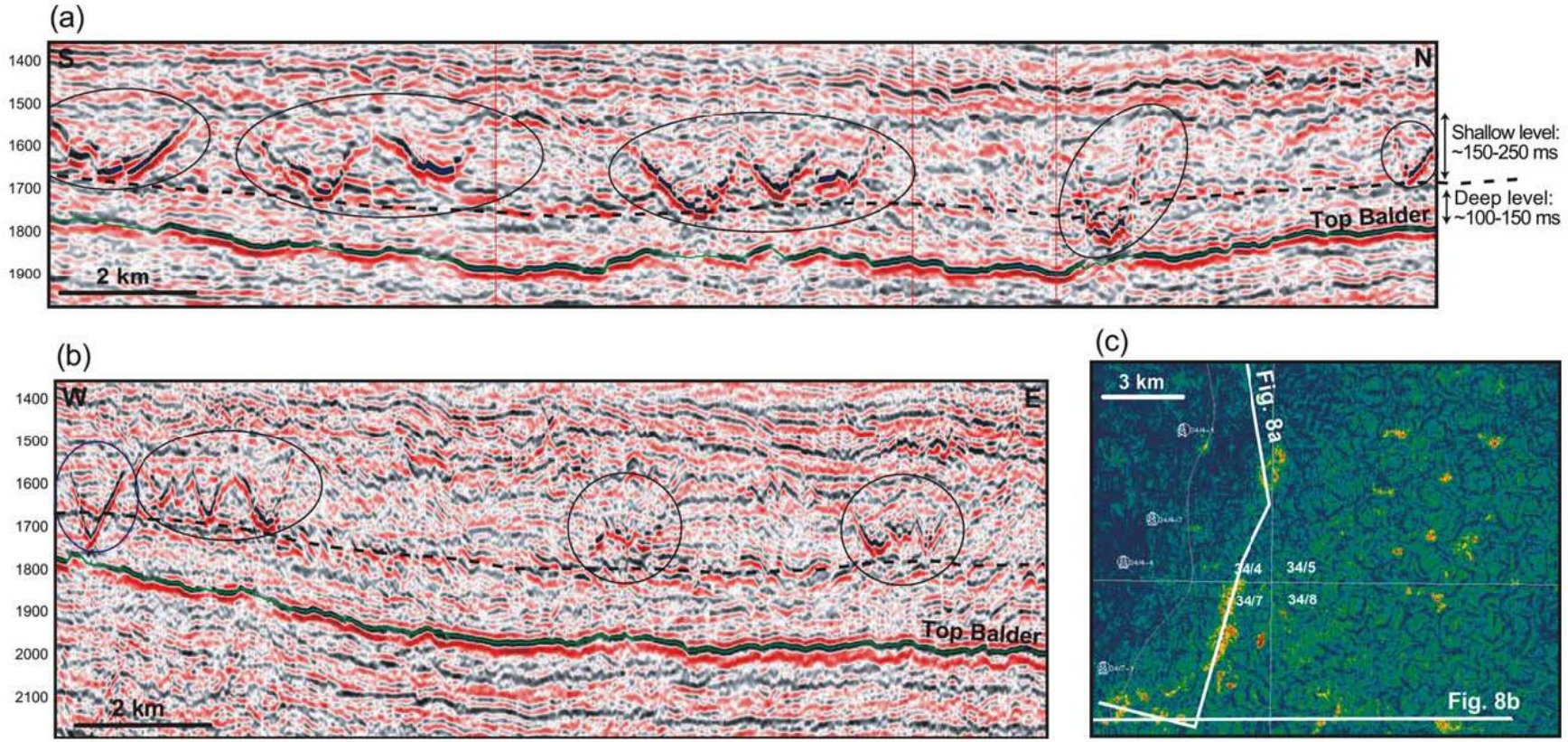

Fig. 8. (a and b) Seismic lines showing two levels of downward termination of the discordant amplitude anomalies. (c) Line location indicated on map of integrated amplitude between 120 and 240 ms TWT above Top Balder.

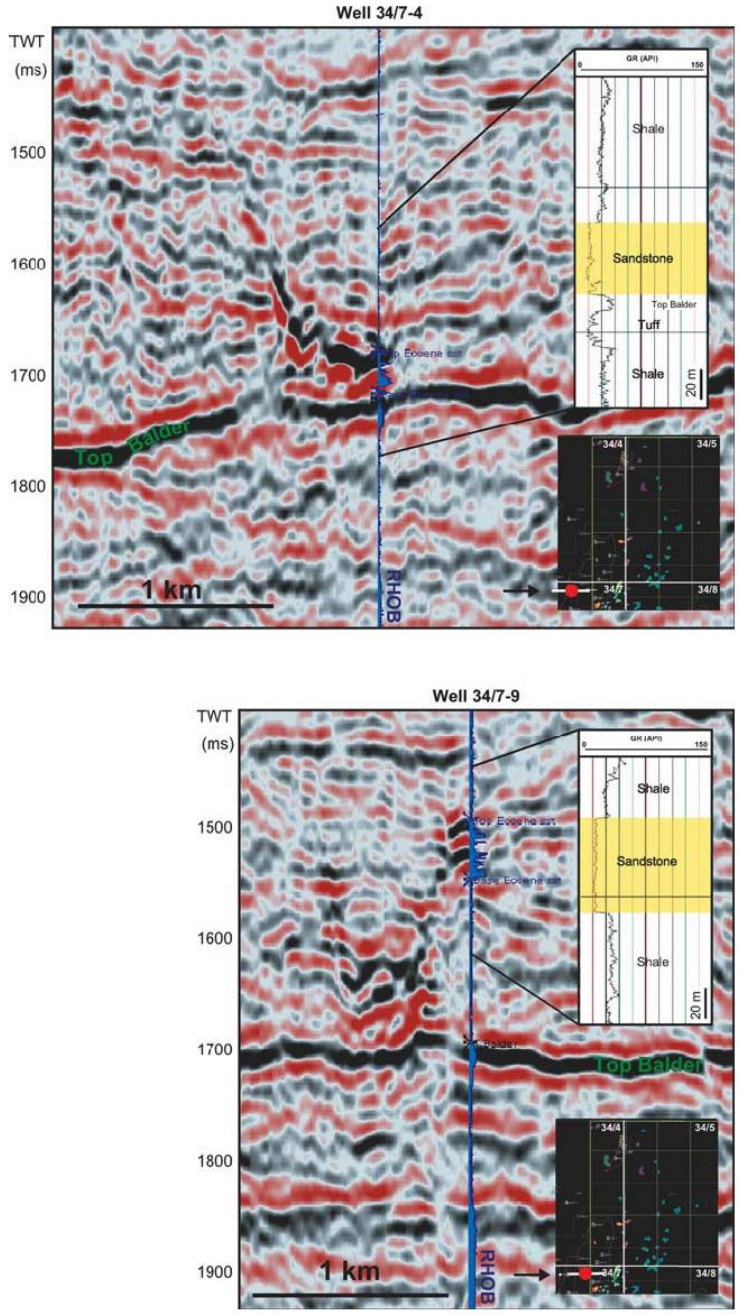

Fig. 9. Well calibration of two discordant amplitude anomalies in Block 34/7 yield some 50–60 m variably cemented sandstone. See text for discussion.

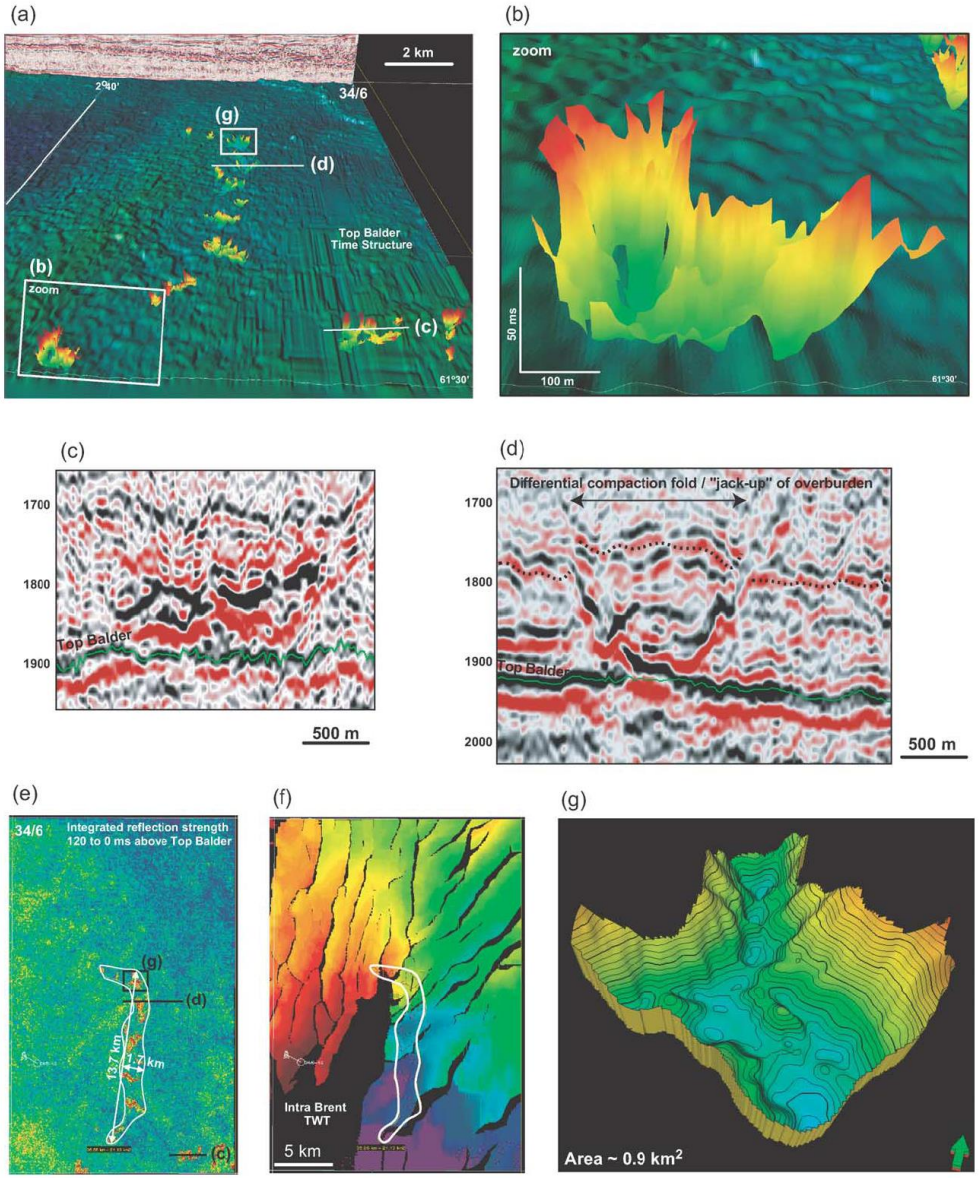

Fig. 10. (a) Three-dimensional visualization of conical amplitude anomalies above the Top Balder surface in Block 34/6. The anomalies occur along the flank of a gentle anticline developed over the crest of a tilted fault block. (b) Individual anomalies may be some hundred metres to over a kilometre wide. The anomaly shown close up is about 100 ms TWT in height. (c and d) The seismic expression of the anomalies is similar to that of remobilised sandbodies further south in the northern North Sea (e.g. Alba: Jones et al., 2003; Grieg: Huuse et al., 2004). (e) The lateral extent of the aligned anomalies is comparable to that of the Alba Field outline, i.e. some 13–14 km length and 1–2 km width. (f) The outline of the anomalies closely follows the flank of the underlying structure represented by the Intra Brent Group TWT-structure. (g) The area of a single conical anomaly may be used to infer potential reservoir volumes, assuming that the anomalies represent sandstone (cf. Fig. 9). The area of the anomaly shown here is about 0.9 km^2, and its height is about 100–125 ms TWT.

Late Cenozoic geological evolution of the northern North Sea: development of a Miocene unconformity reshaped by large-scale Pleistocene sand intrusion

H. Løseth, B. Raulline and A. Nygård

Journal of the Geological Society, 170, 133-145, 4 January 2013, https://doi.org/10.1144/jgs2011-165

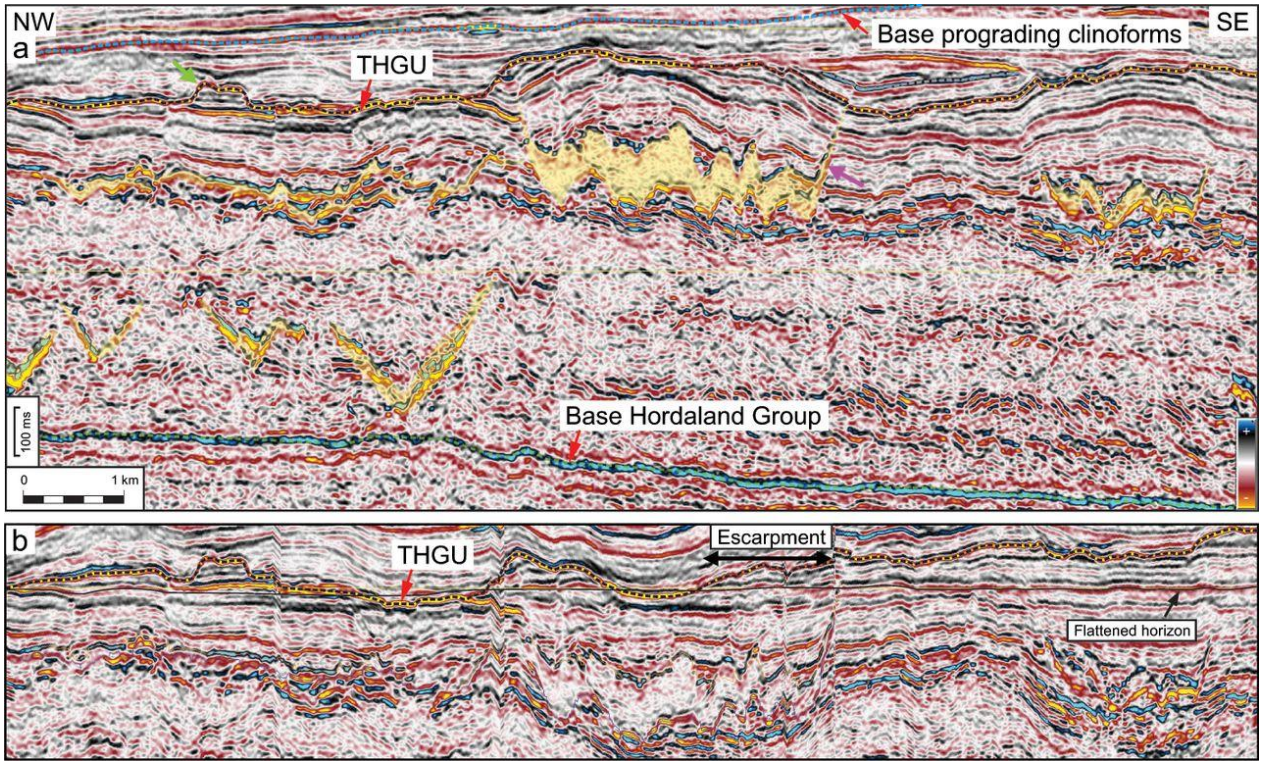

Fig. 8. NW–SE-striking seismic section crossing the high mound at the top Hordaland Group unconformity (THGU) above the Visund Field and underlying sand injectites (yellow overlay) (location shown in Fig. 5). Irregular zigzag-shaped peak and trough reflections are *c.* 200 ms below the top Hordaland Group unconformity and well ties place them at the top and base of sands. (**b**) The same section as in (**a**) but flattened on an intra Hordaland Group horizon in (**a**). The flattening removes the mounds that were formed when sand was injected. Such flattening restores the pre-injection erosive shape of the top Hordaland Group unconformity. An erosive outlier is observed at the green (westernmost) arrow.

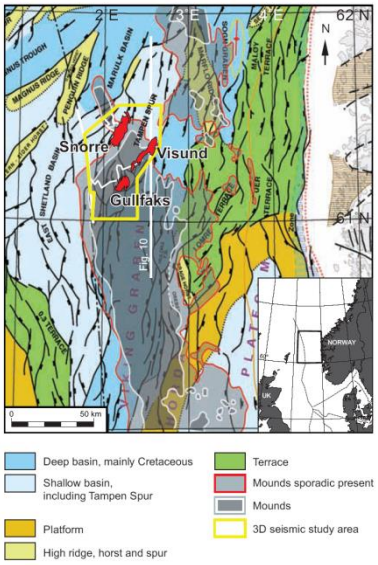

Late Cenozoic geological evolution of the northern North Sea: development of a Miocene unconformity reshaped by large-scale Pleistocene sand intrusion

H. Løseth, B. Raulline and A. Nygård

Journal of the Geological Society, 170, 133-145, 4 January 2013, https://doi.org/10.1144/jgs2011-165

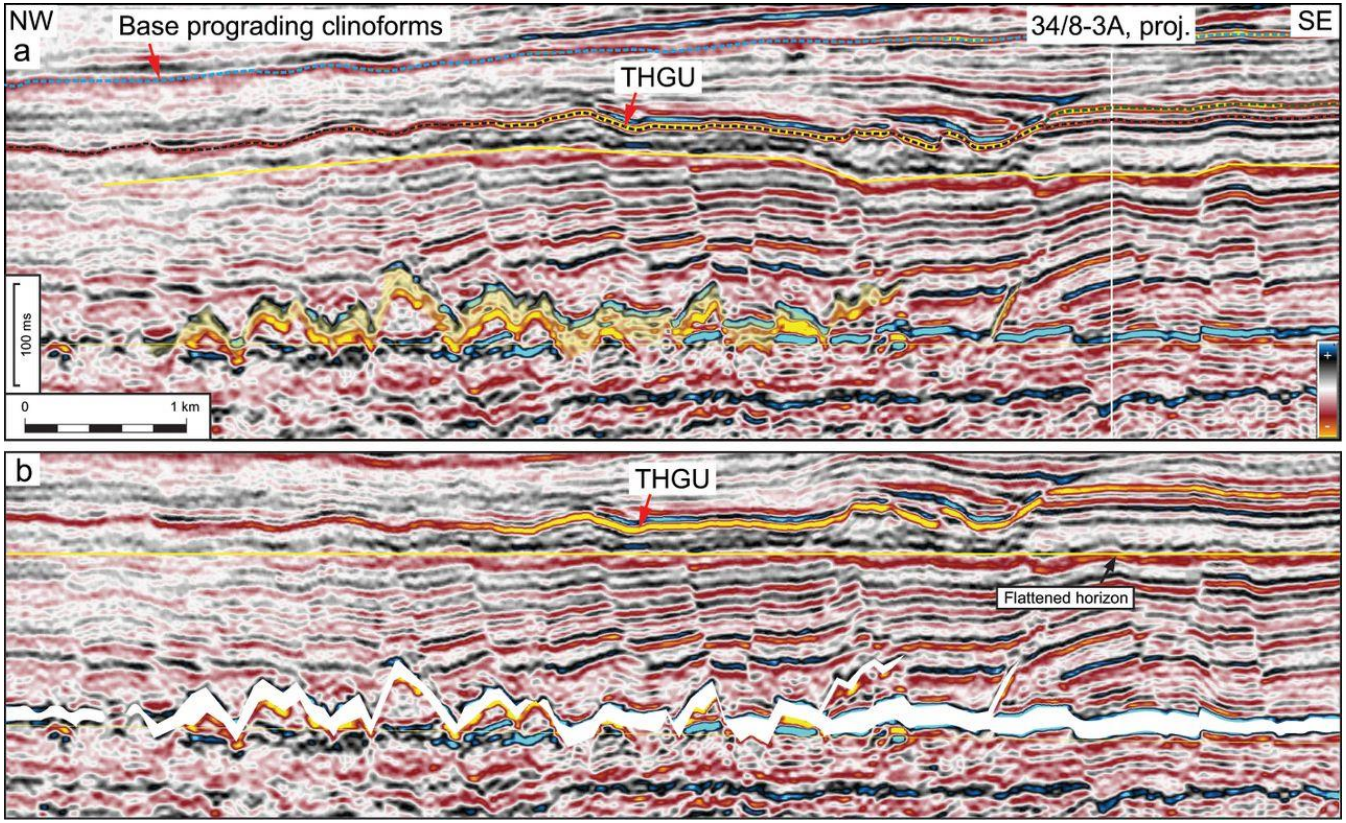

Fig. 7. (**a**) NW–SE-striking seismic section showing the escarpment at the top Hordaland Group unconformity (THGU) just south of well 34/8-3A and an underlying sand injectite (yellow overlay) (location in Fig. 5). Zigzag-shaped peak and trough reflections, which tie to the top and base of sands in nearby wells, can be observed *c*. 200 ms below the top Hordaland Group unconformity. (**b**) The same section as in (**a**) but flattened on the intra Hordaland Group yellow horizon in (**a**). The flattening removes the smooth mound that was formed above the injected sand. The flattened section is cut at the top sand reflection whereas the lower part of (**b**) is the lower part of (**a**) cut at the base of the sand. Together, they show a reconstruction of the Hordaland Group before the sand was injected. The reconstruction is validated by the gap between the two parts being almost equally thick.

Late Cenozoic geological evolution of the northern North Sea: development of a Miocene unconformity reshaped by large-scale Pleistocene sand intrusion

H. Løseth, B. Raulline and A. Nygård

Journal of the Geological Society, 170, 133-145, 4 January 2013, https://doi.org/10.1144/jgs2011-165

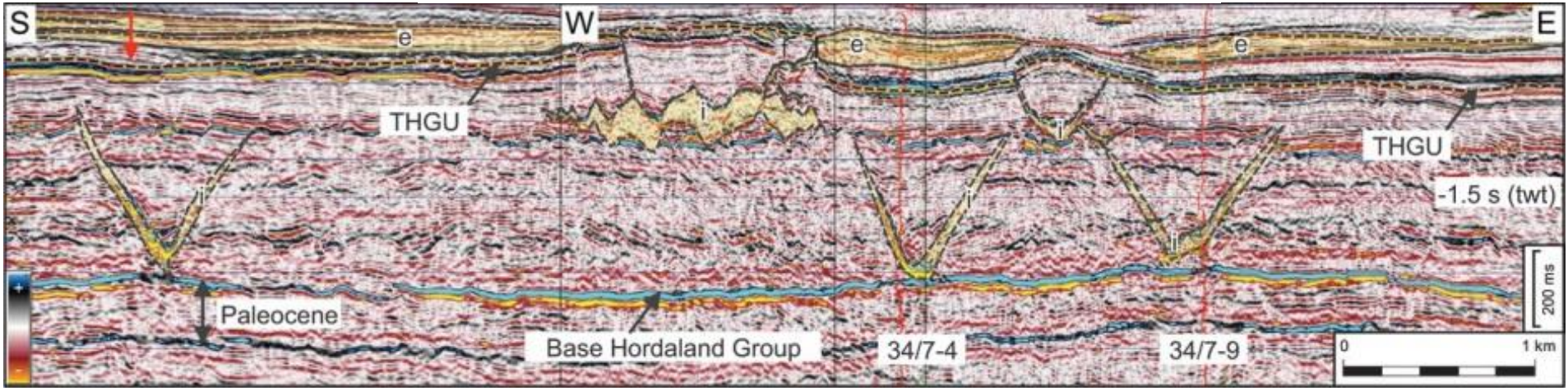

Fig. 12. Seismic section through wells 34/7-4 and 34/7-9 showing intrusive (i) and extrusive (e) sands, expressed as low gamma-ray readings (red curve), above the Snorre Field (location in Fig. 6). The deep V-shaped bright anomalies in the lower part of the Hordaland Group are partly carbonate-cemented sand injectites. The parent sands for the injectites and extruded sands are interpreted as turbitides originally deposited in the Palaeocene interval. The feeder (f) from the intrusive sand to the extrusive sands should be noted. The red arrow points to the subtle depression at the top Hordaland Group unconformity (THGU) that is located above an intrusive sand.

Geology, May 2012; v. 40; no. 5; p. 467–470; doi:10.1130/G33117.1; 4 figures; Data Repository item 2012133.

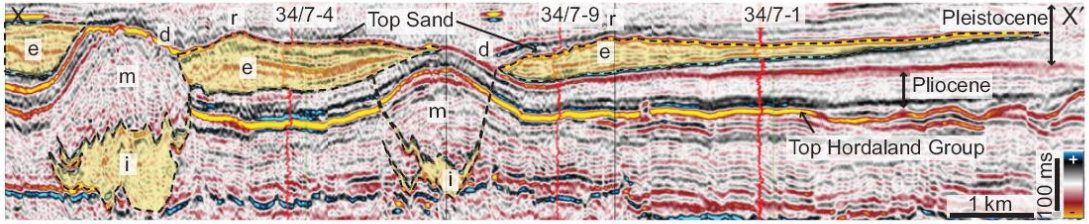

Figure 2. Interpreted seismic section across study area, showing sandbodies (yellow overlay). (For line of section X–X′, see Fig. 1.) Vertical scale (in ms, two-way traveltime) is ~5 times horizontal scale (in km). Sand has low gamma-ray readings on wire-line well logs (red traces). Wells 34/7–4, 34/7–9, and 34/7–1 (green lines show position) penetrated 82 m, 57 m, and 24 m of sand, respectively. Interpreted body of extrusive sand (e) onlaps and wedges out away from ditches (d) toward top of mound (m), which formed when high fluid pressure jacked open fractures and filled them with intrusive sand (i). Removing this sand and closing gap by a model of simple vertical shear results in almost flat surface for top of Hordaland Group. Ridges (r) at top sand surface are east of ditches.

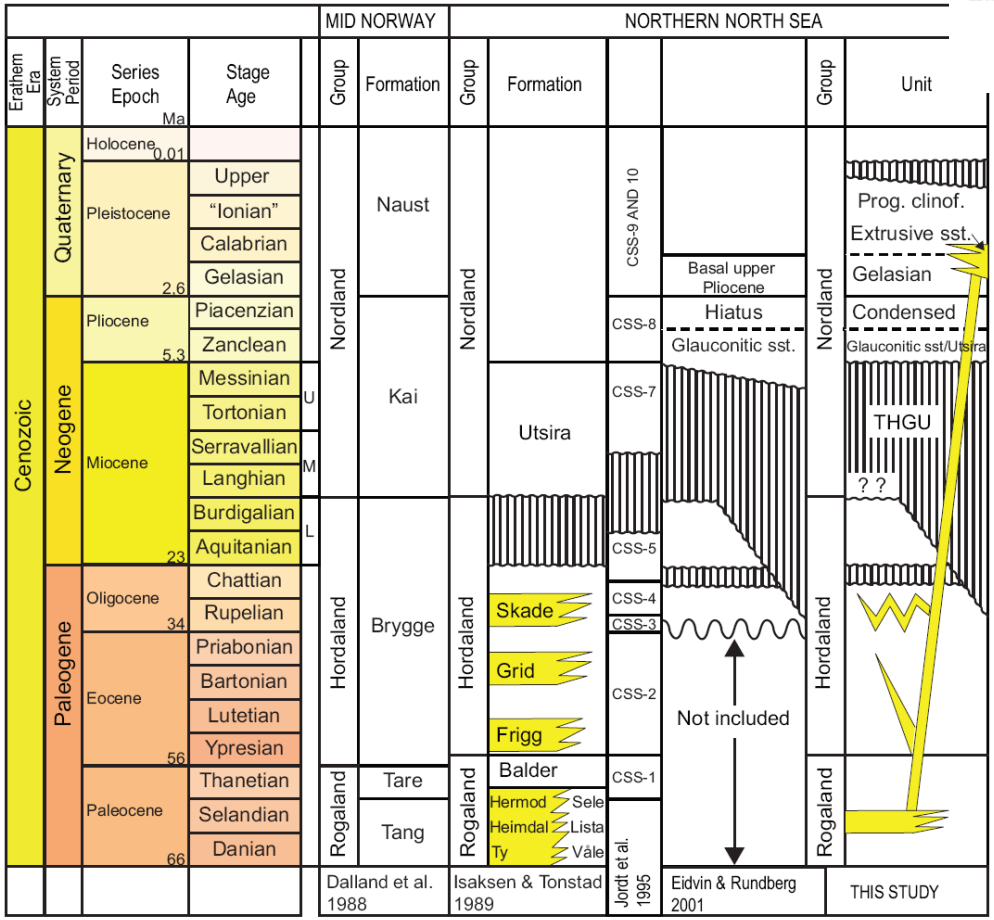

Fig. 2. Summary of stratigraphy in mid-Norway and the northern North Sea. Age assigned to the top Hordaland Group unconformity (THGU) and Utsira Formation, which is partly time equivalent to the glauconitic sand in the study area, varies from early Miocene to Pliocene in completion logs and the literature owing to large amounts of re-sedimented fossils. Stratigraphic positions of intrusive and extrusive sands are shown. The time scale is from Ogg 2010.

Late Cenozoic geological evolution of the northern North Sea: development of a Miocene unconformity reshaped by large-scale Pleistocene sand intrusion

H. LØSETH[1]*, B. RAULLINE[2] & A. NYGÅRD[2]

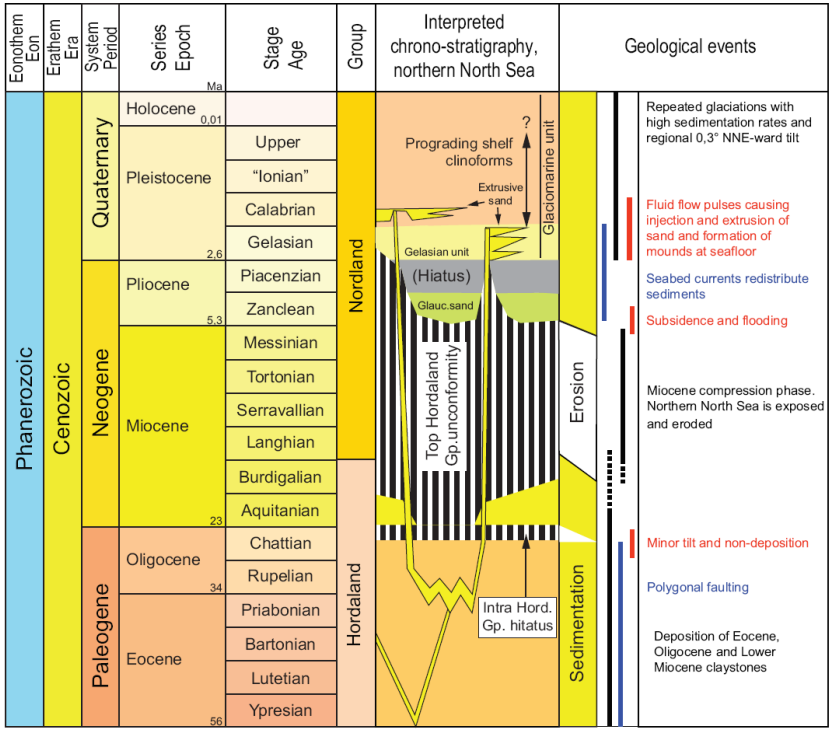

Fig. 15. Summary of interpreted chronostratigraphy and geological events in the northern North Sea during the late Cenozoic.

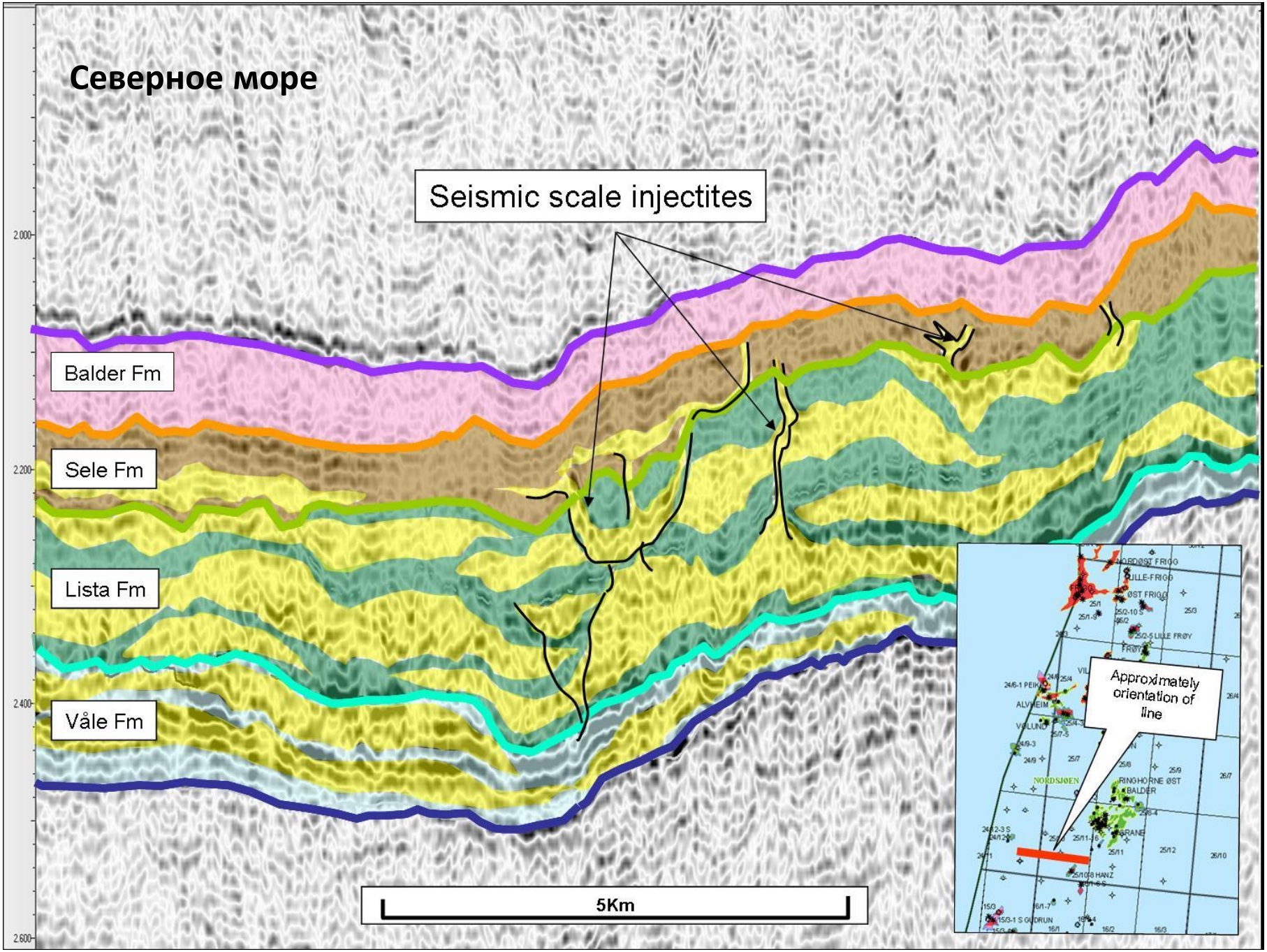

Example of seismic scale injectite systems in the southern parts of block 25/10.

Tertiary deep-marine reservoirs of the North Sea region: an introduction

T. McKie, P. T. S. Rose, A. J. Hartley, D. W. Jones and T. L. Armstrong

Geological Society, London, Special Publications, 403, 1-16, 20 August 2015, https://doi.org/10.1144/SP403.12

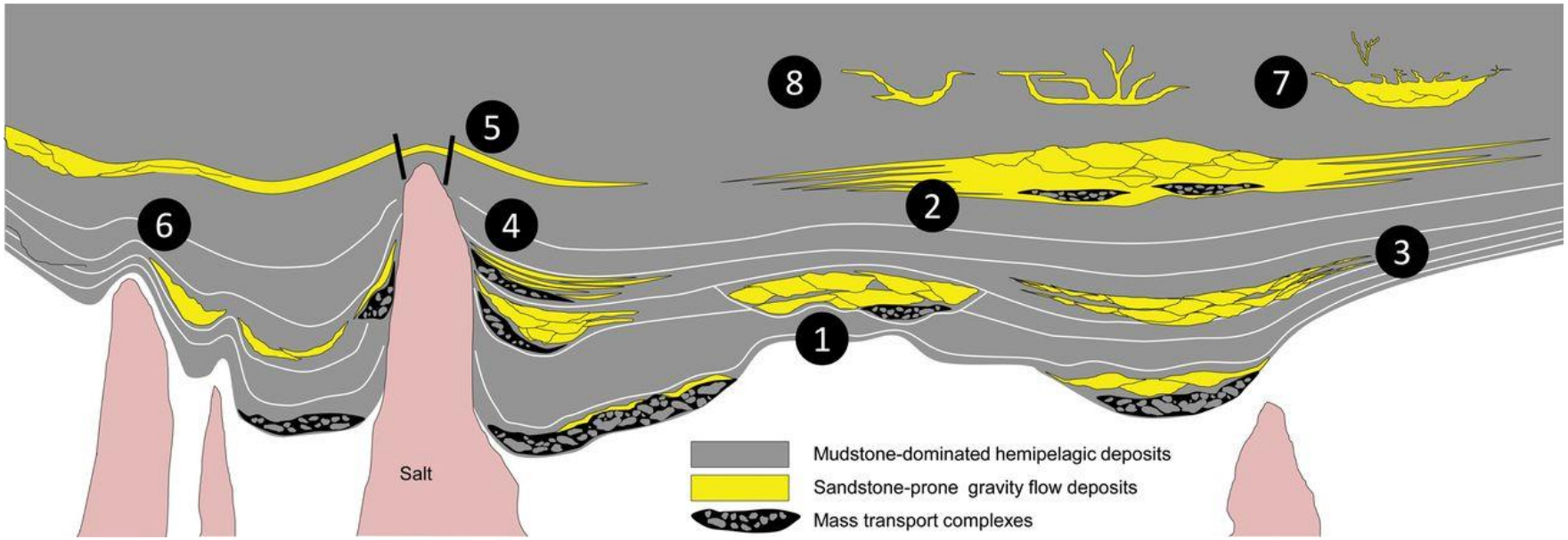

Trapping styles of deep-marine reservoirs in the North Sea region: 1, compactional relief over basement highs (e.g. the channelized Forties and Nelson fields); 2, large-scale compactional relief of the fan system (e.g. the Frigg Field); 3, fan-fringe onlap of basement highs (e.g. the Everest and Arran fields); 4, diapir piercement structures and associated channel and lobe-filled rim synclines (e.g. the Pierce, Merganser and Fram fields); 5, uplifted and domed reservoirs largely deformed post-deposition (e.g. the Scoter and Starling fields); 6, minibasin traps with confinement by salt structures and antecedent fans (e.g. the Gannet A and Bittern fields); 7, partially remobilized sandbodies with trapping reliant on mechanisms 1–6, but with reconfigured geometry (e.g. the Alba Field); 8, reservoirs entirely consisting of injected dykes and sills (e.g. the Volund Field).

Северная Атлантика, Шетландские острова-Фареры

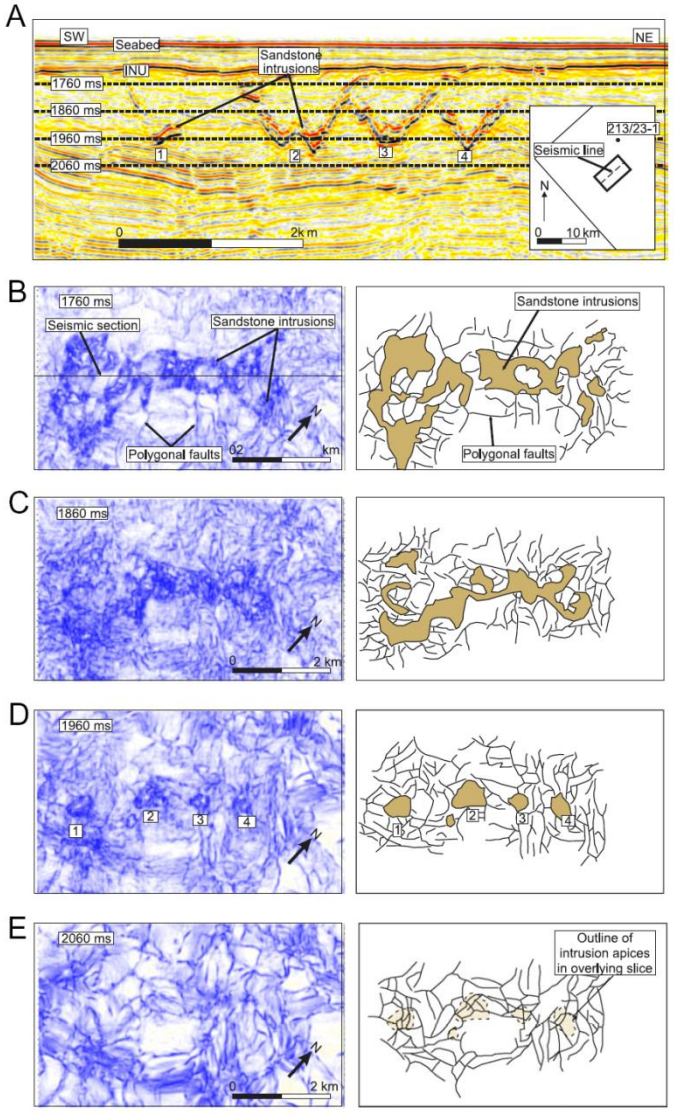

Fig. 6. (A) Seismic section through a series of orphan conical sandstone intrusions with no observable feeder system. Note the range of different apex geometries including pointed, rounded and flattened or bowl-shaped. Depth of variance slices marked with dashed lines. (b–e) Variance slices every 100 ms through the polygonally faulted section containing the sandstone intrusions with an interpretation of the variance slice to the right (sandstone intrusions are marked in pale brown). Note how polygonal faults have a well-defined linear character while sandstone intrusions have a more globular texture. (D) Intrusion apices are closely related to fault intersections. (E) No evidence of a feeder system can be seen in the polygonally faulted section below the conical sandstone intrusions

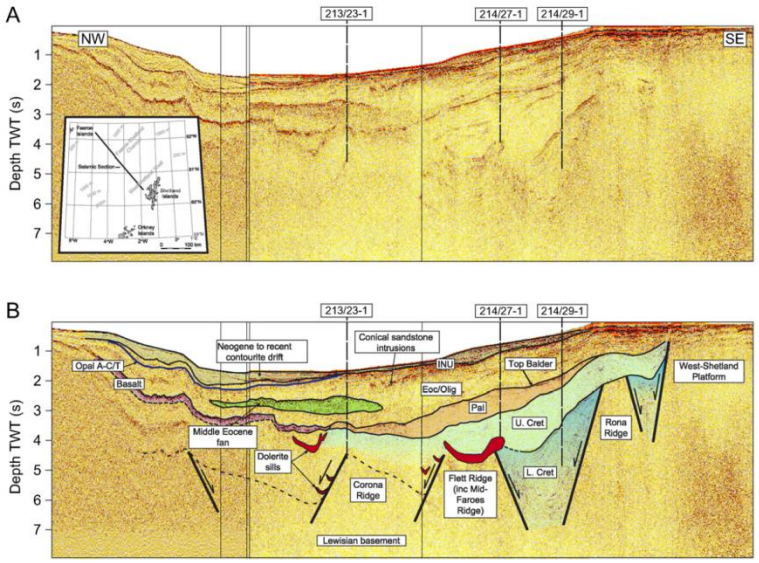

Fig. 2. (A) Regional 2D seismic line across the Faroe-Shetland Basin tied to three exploration wells. (B) An interpreted seismic line across the Faroe-Shetland Basin showing the major basement fault blocks and overlying sedimentary strata.

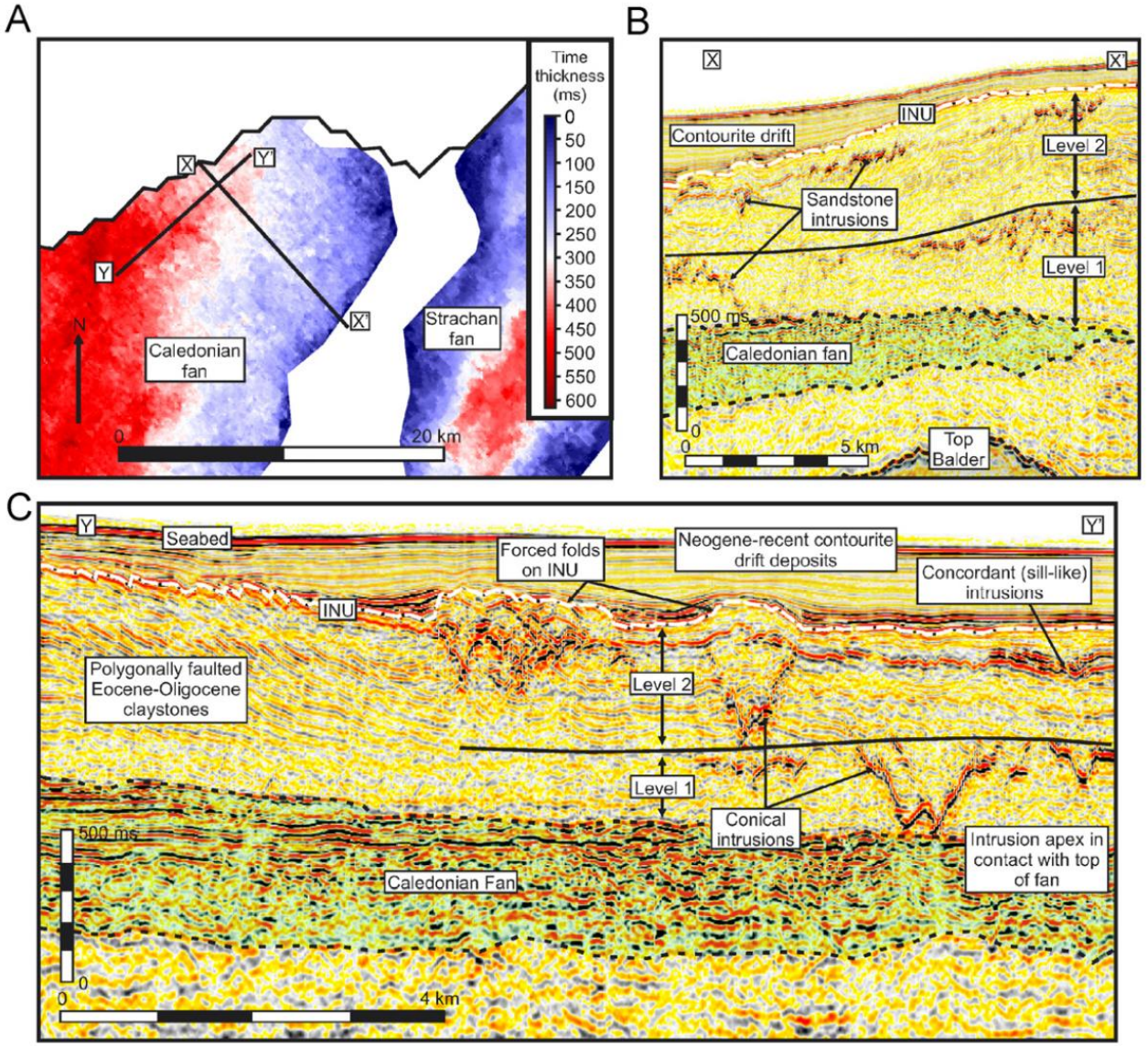

Fig. 7. (A) Location map showing the position of seismic lines X–X′ and Y–Y′ relative to isochrons of the Caledonian and Strachan fans. (B) Seismic line X–X′ showing the position of two-tier sandstone intrusion network within the Eocene–Oligocene succession relative to the Caledonian fan and an underlying high on the Top Balder surface. This high represents the Corona Ridge Fault block. (C) Conical sandstone intrusions in the basal tier of the intrusion network are physically linked to the Caledonian fan. The top of tier 1 is marked by a series of concordant high-amplitude reflections likely to represent sandstone sills. Conical sandstone intrusion within tier 2 is physically linked to the flat lying intrusions that mark the top of tier 1. Conical sandstone intrusions in tier 2 propagate upwards as far as the INU and cause uplift of the INU surface.

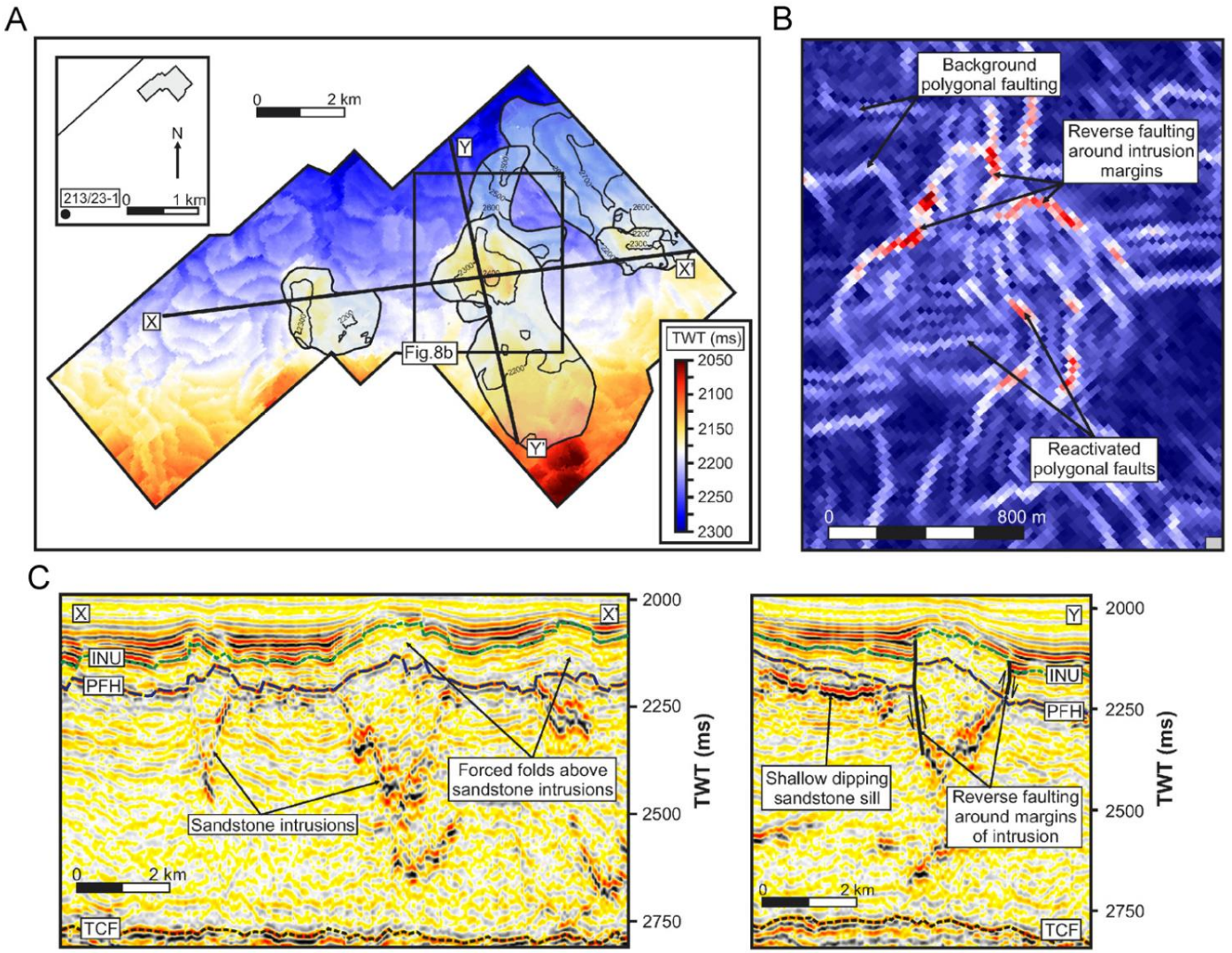

Fig. 8. (A) Depth map of a polygonally faulted horizon below the INU (blue dashed line, Fig. 8c) with the position of underlying intrusions overlain. Local sub-circular highs on the mapped surface are closely spatially related to shallow conical sandstone intrusions. (B) A dip map of the mapped surface above a shallow conical sandstone intrusion reveals that uplift above shallow intrusions is accommodated by the reactivation of the pervasive polygonal fault network and by the formation of reverse faults around the margins of the intrusion. (C) Seismic sections through the mapped region: X–X′ Shallow intrusions, underlain by deeper feeder intrusions, cause the uplift of the INU surface (green dashed line). Maximum uplift occurs above the thickest parts of the underlying intrusion (usually the apex) and the resultant extension of the overlying block is taken up by the reactivation of pre-existing polygonal faults. Note the presence of high-amplitude packages of post-INU contourite drift strata that onlap the mounded geometry on the INU formed as a result of intrusion and uplift. Y–Y′ Uplift of strata overlying a shallow intrusion is not just facilitated by extension of the overlying strata, but also by the formation of reverse faults around the margins of the shallow intrusion.

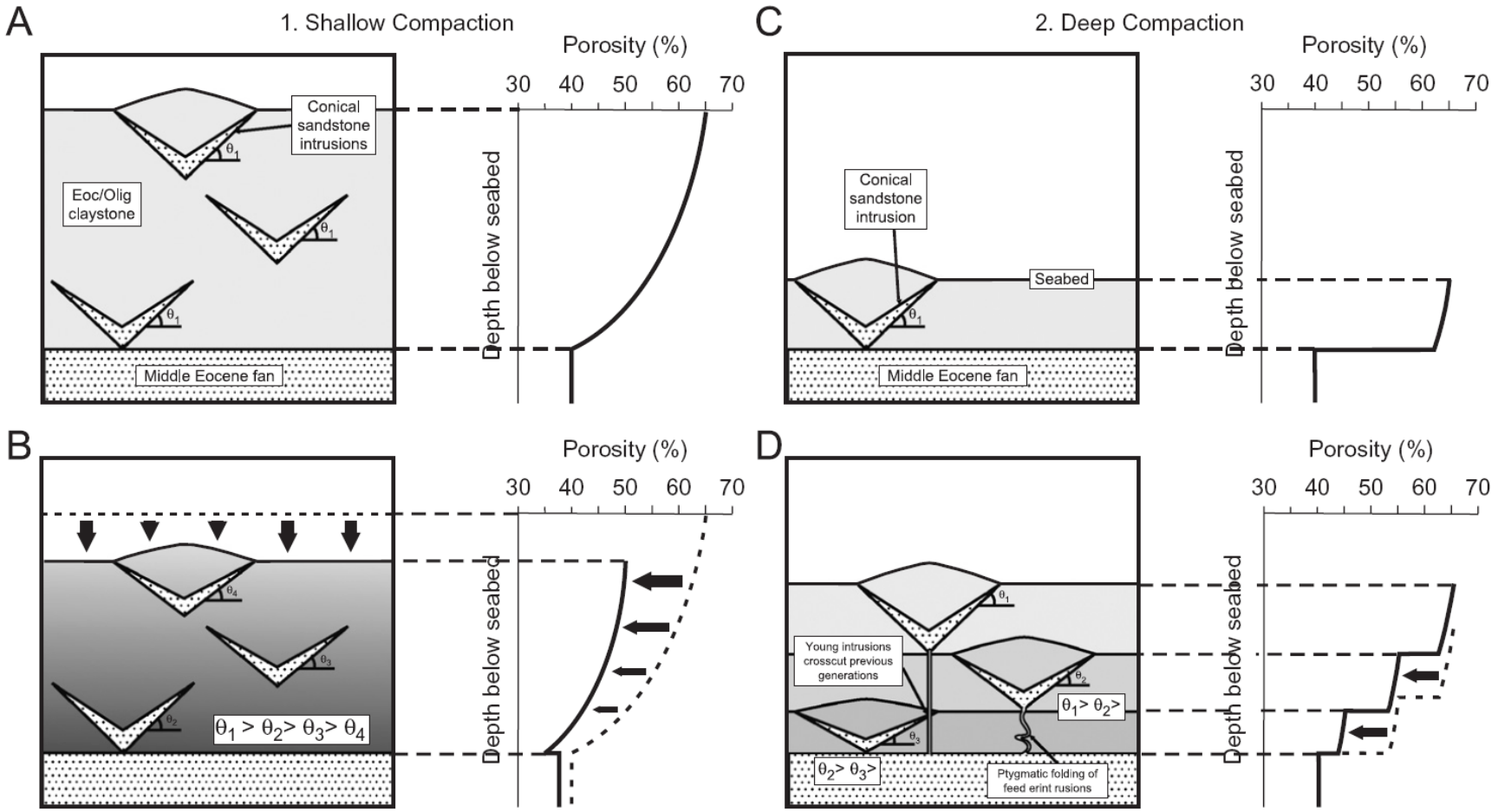

Fig. 10. Two schematic models to explain the relationship between intrusion angle and compaction. (A) Conical sandstone intrusions are intruded throughout a semi-compacted host rock sequence in a single intrusion event. (B) After the emplacement event, compaction of the host rock sequence continues. The greatest levels of compaction will occur at shallow levels where host rock porosity is greatest. Thus shallow sandstone intrusions will suffer the greatest levels of flattening due to compaction. (C) Conical sandstone intrusions are intruded in a series of temporally separate episodes. (D) Subsequent deposition and emplacement episodes result in further compaction of the preexisting host rock sequence. Thus the discordant limbs of older intrusions will have more shallow dips than younger intrusions. It is also likely that later intrusive events will crosscut preexisting sandstone intrusions and that the feeder systems of older intrusions will become folded as a result of compaction of the host rock sequence.

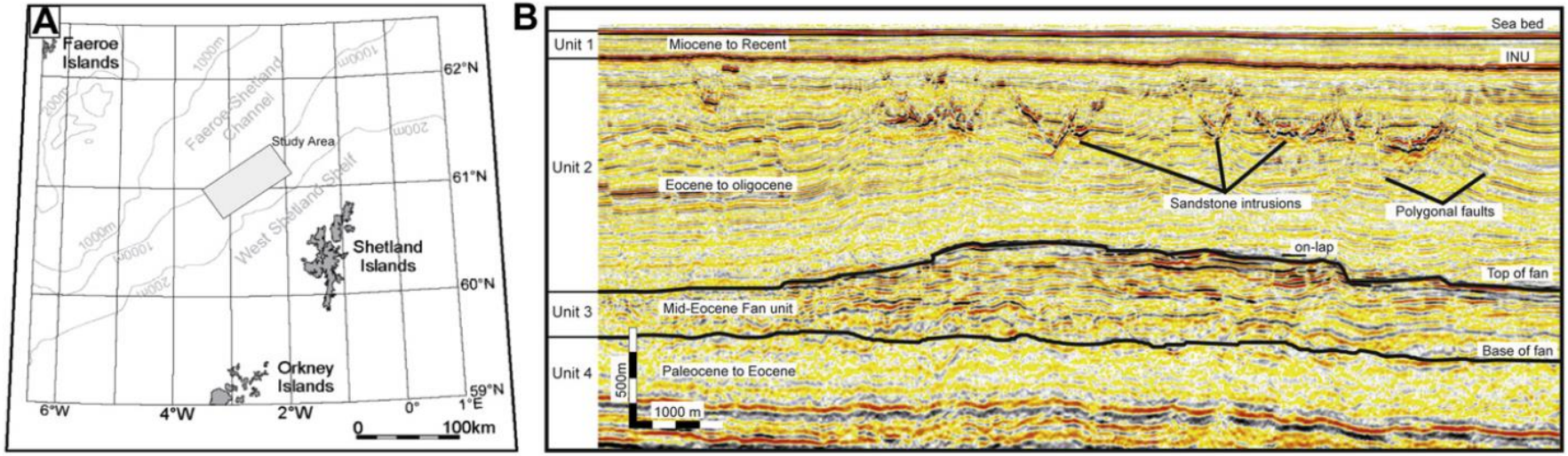

Fig. 1. A: Location map. Study area located within area of three-dimensional seismic data (grey box). B: Seismic section showing stratigraphy of Paleocene to Holocene strata divided in different units. V-shaped high amplitude reflections in the Eocene–Oligocene sequence are interpreted as conical sandstone intrusions within a polygonally-faulted interval, overlying the Middle Eocene fan unit. INU = Intra Neogene Unconformity.

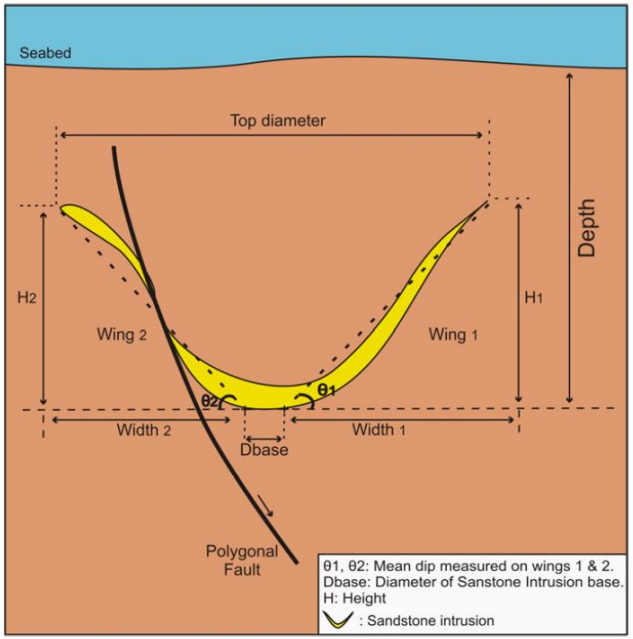

Fig. 2. The notation used for sandstone intrusion characterisation.

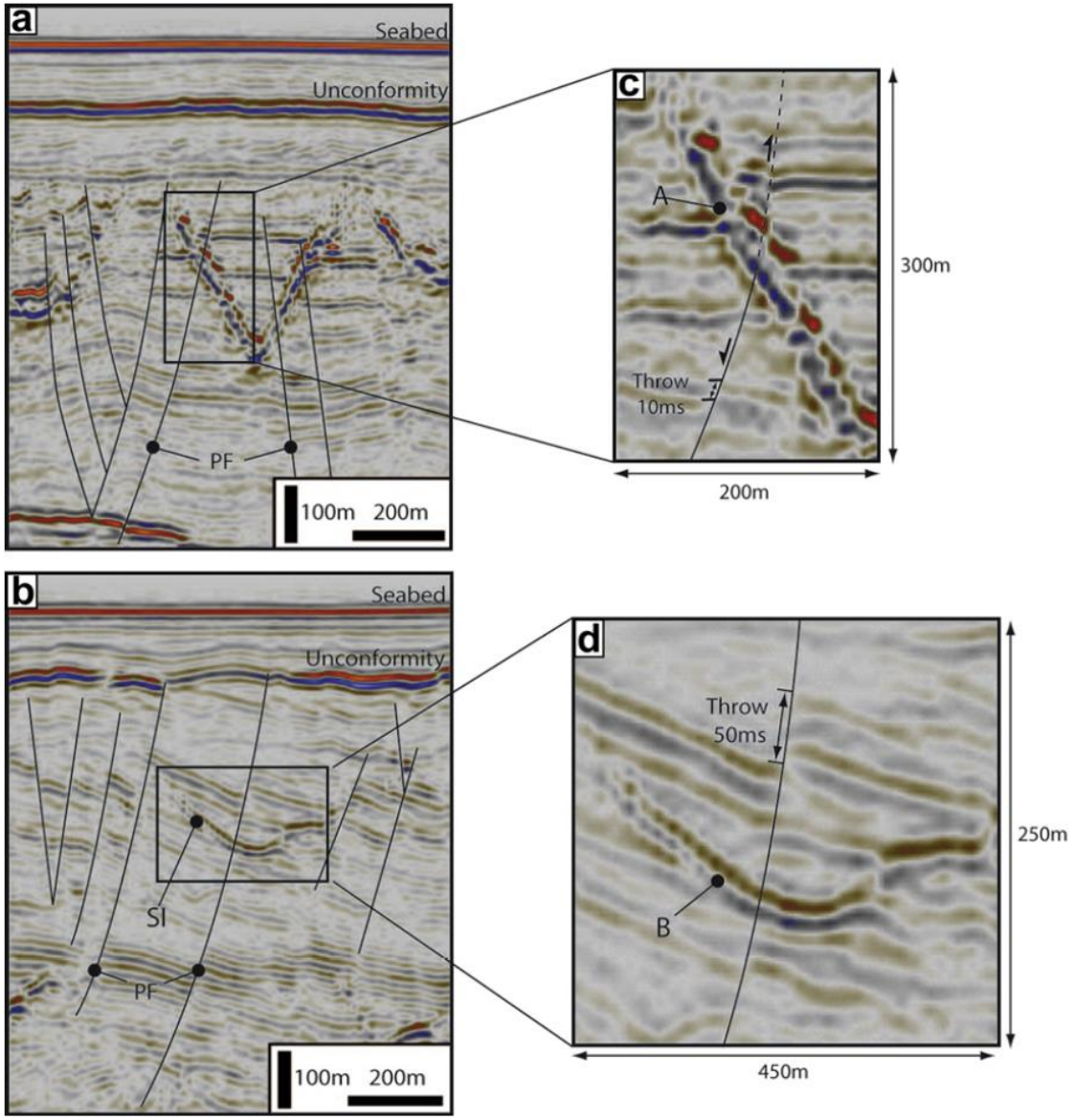

Fig. 3. Seismic expression of sandstone intrusions that crosscut or are unaffected by polygonal fault planes (Type 1). (a) and (b) are two good examples of sandstone intrusions with different thicknesses crosscut by faults but geometrically unaffected. (c) and (d) represent zooms of these intrusions which are not affected by low or high-throw faults respectively (intrusion A and B).

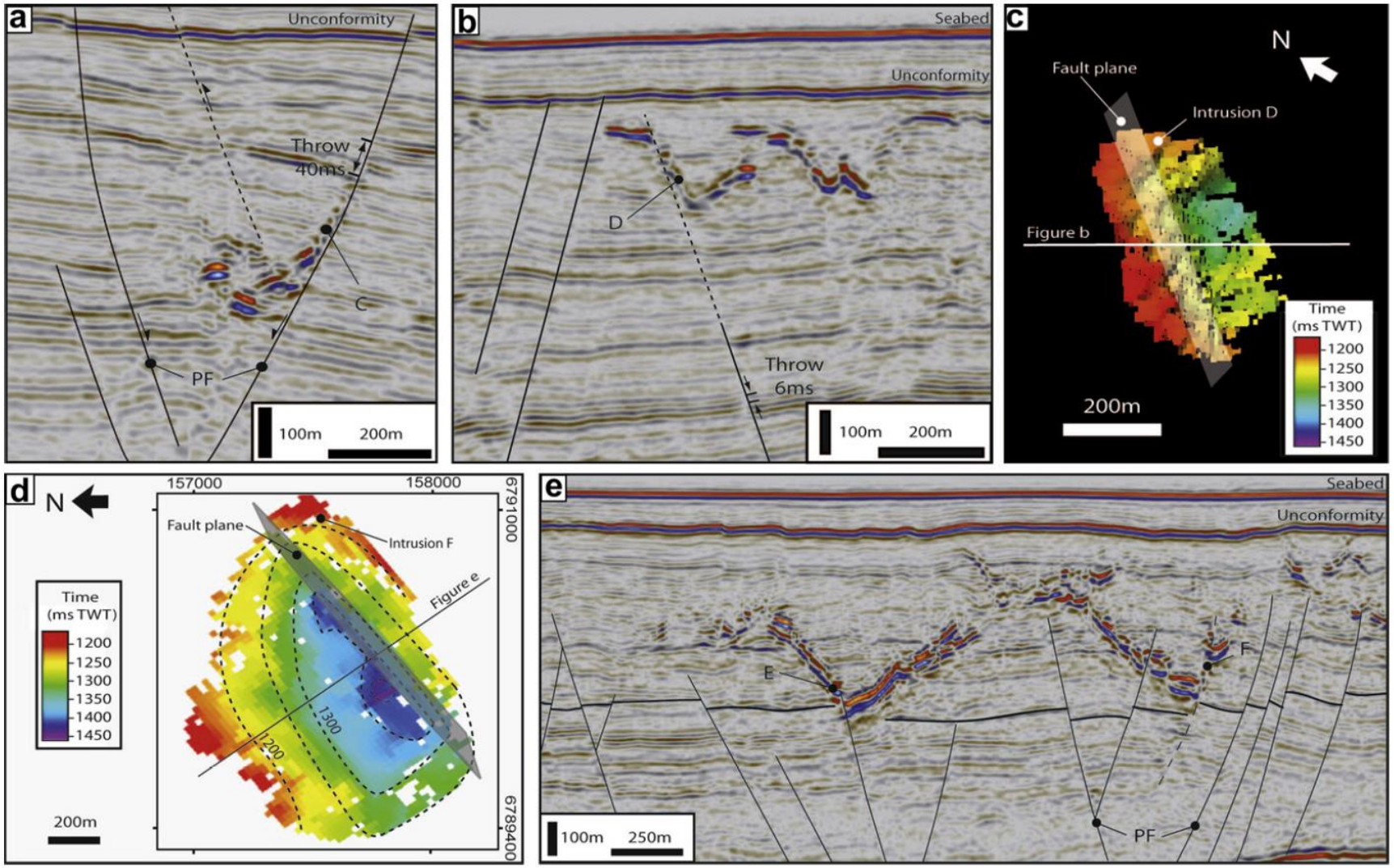

Fig. 4. Detailed seismic and 3D expression of Type 2 sandstone intrusions intruded along polygonal fault planes. Type 2a is highlighted on Figure a, Type 2b is detailed on Figures b, c, d and e. (a) Example of half conical sandstone intrusion (C), where one flank is completely following a polygonal fault. Note that this polygonal fault is characterized by a great value of throw (≈40 ms). (b) Example of an intrusion limb D following a fault with small throw (6 ms in depth). Intruded fault trace is unclear in between 500 and 150/200 m but evidences shows that it progressively dies out. Intrusion D goes out of the fault upwards. (c) 3D view from the top of intrusion D with the position of fault plane responsible of the formation of western abrupt margin. (d) TWT map of Intrusion F (Fig. e) showing a limb slope greater when intrusion flank uses fault plane. Note that the 3D geometry of this intrusion is clearly controlled by the occurrence of fault plane. (e) Examples of asymmetric forms (intrusions E and F), where one flank is partially intruded along fault plane.

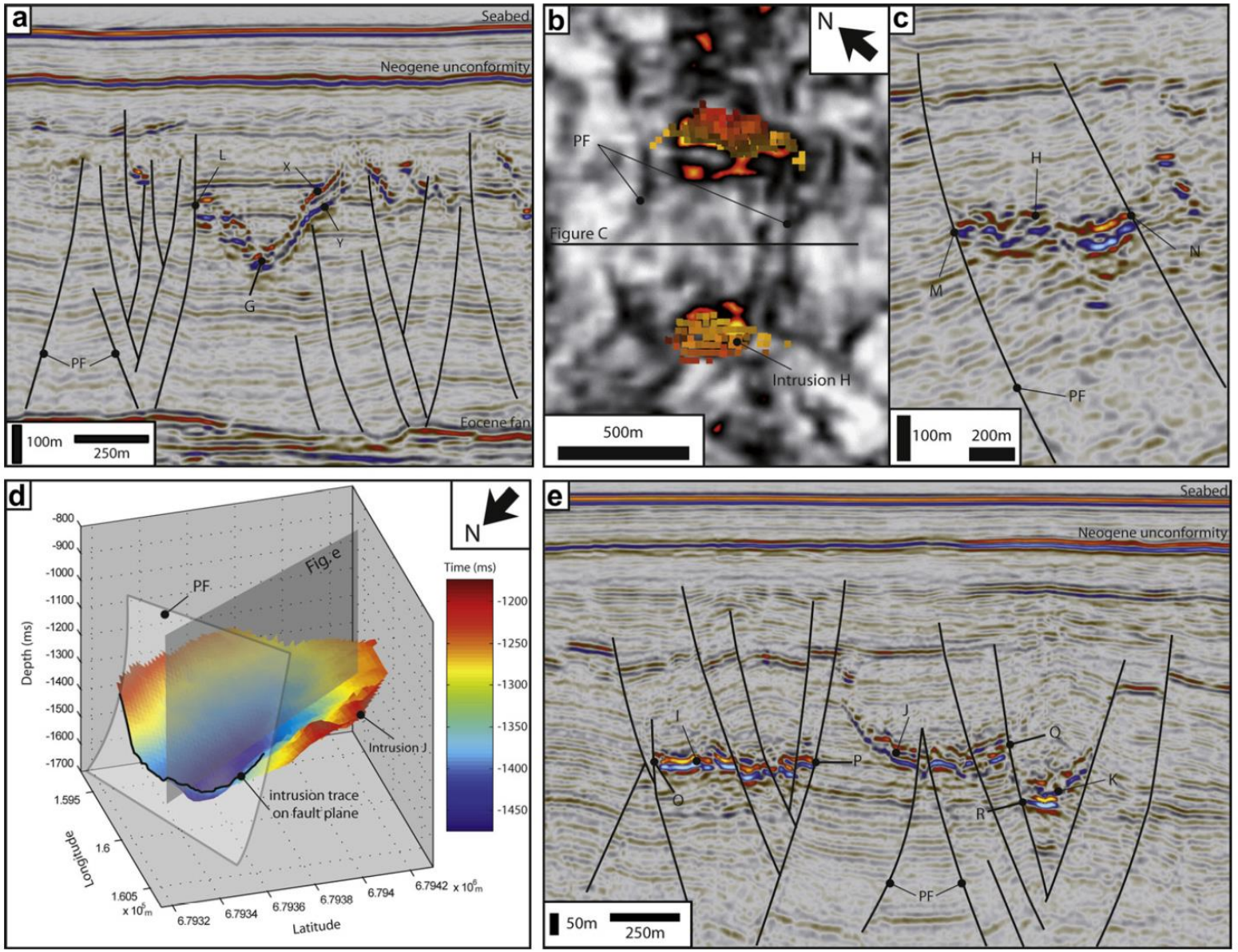

Fig. 5. Seismic characterization of sandstone intrusions arrested by faults in Faroe-Shetland basin (Type 3). (a) Representative seismic line showing a conical amplitude anomaly (Intrusion G) with one flank arrested by a fault. (b) Variance slice in the middle of a gutter-shaped sandstone intrusion showing two polygonal faults oriented ≈N045°E controlling lateral extending of Intrusion H. (c) Seismic expression of intrusion H showing tow arrested-points (M, N) against faults on each side of the intrusion. (d) 3D view of intrusion J (Fig. e) showing interaction between fault and sandstone intrusion with intrusion trace on fault plane. (e) Seismic profile across several intrusions (I, J and K) and arrested-points (O, P, Q and R).

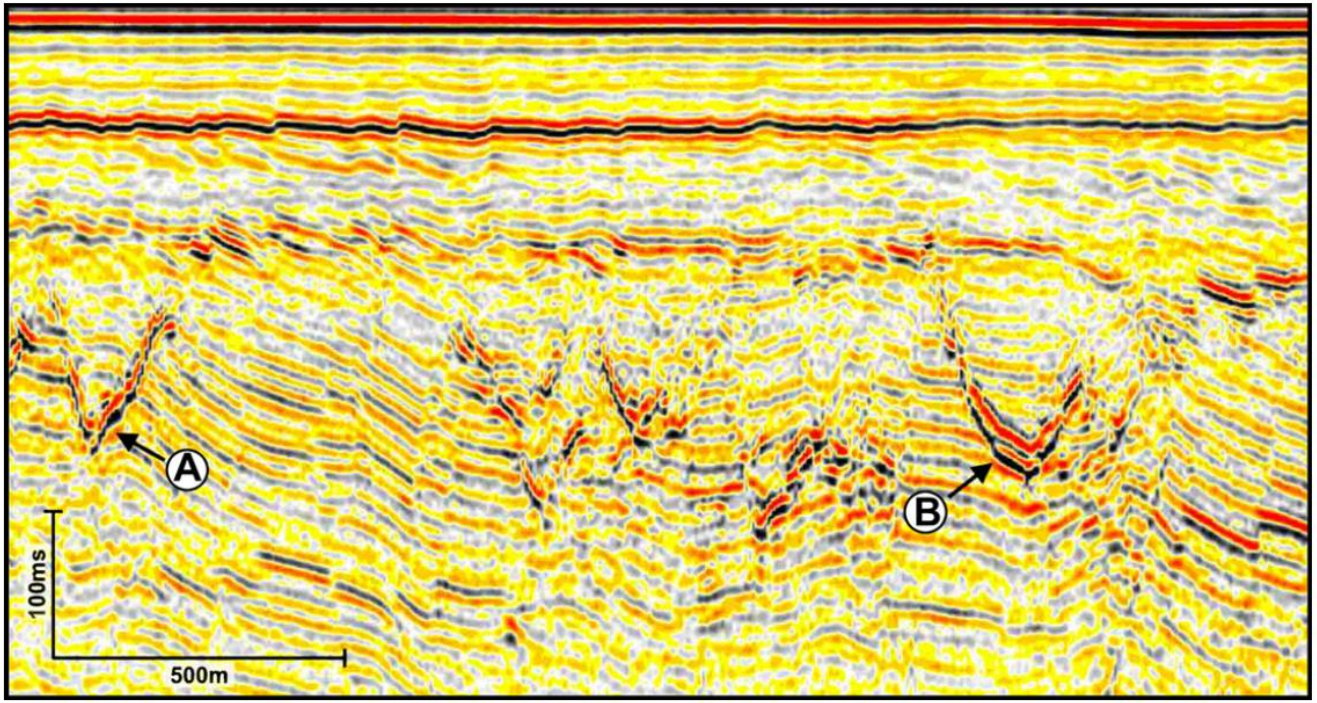

Fig. 2. Seismic expression of conical sandstone intrusions. This profile is from the Faeroe–Shetland Basin, and shows a number of discordant, 'v-shaped' high amplitude reflections with either sharp apices (A) or blunt-based apices (B). These are interpreted as sandstone intrusions within a polygonally-faulted host sequence of Eocene claystone. Note the large variety of cross-sectional geometry, from symmetrical to asymmetrical, singular to composite. Data courtesy of Exxon-Mobil Ltd.

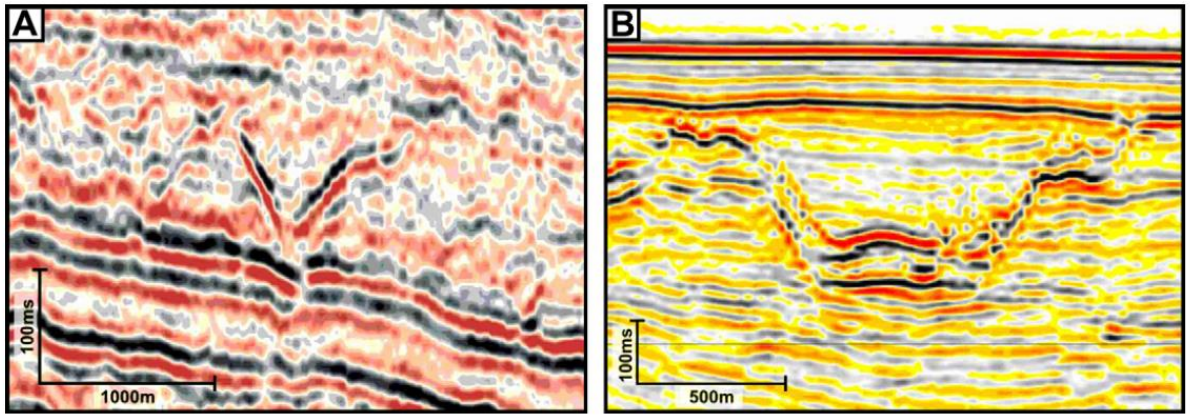

Fig. 3. End members of the spectrum of large-scale conical sandstone intrusions. (A) Apical cones, with sharp apices and inward dipping flanks typically ranging from 20 to 40 ° (from Molyneux et al., 2002). (B) Flat-based bowls, with concordant basal sheets connected to inward dipping flanks similar in scale and range of dip to those flanking apical cones. Data courtesy of Exxon-Mobil Ltd.

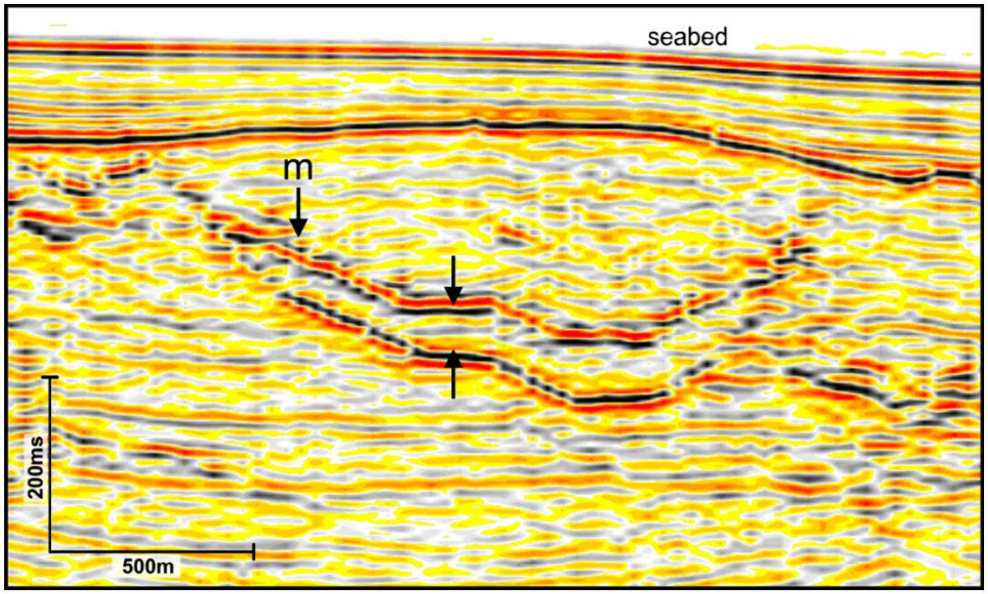

Fig. 8. Seismic expression of a bowl-shaped sandstone intrusion from the Faeroe–Shetland Basin showing the well resolved opposite polarity reflections from the top and base of the intrusion (arrowed). These clearly define the stepped base of the bowl, show the systematic stepping of top and base, and indicate a thinning of the intrusion towards the tips. The details of this wedge-like thinning are partially obscured by multiple reflections (*m*). Also clearly imaged is the forced fold expressed in the strong reflection located c. 100 ms below the seabed. Data courtesy of Exxon-Mobil Ltd.

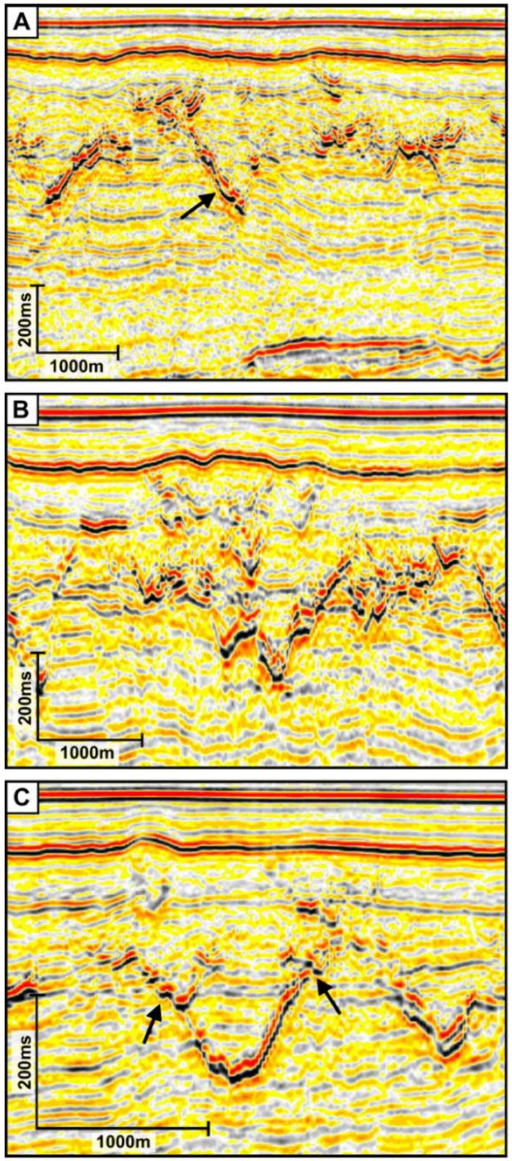

Fig. 6. Detailed seismic expression of apical cones with examples from the Faeroe–Shetland Basin. (A) Example of asymmetric forms, where one flank is better developed because of interactions with pre-existing faults. (B) Example of complex composite form, with many intersections between discordant segments. These can be seen by tracing discordant reflections from pronounced apices upwards into abutting relationships. (C) Example of upward splaying towards the upper tips (arrowed) of a symmetrical form. The splays are easily seen by tracing single high amplitude reflections and noting that they split into two separate reflections. Data courtesy of Exxon-Mobil Ltd.

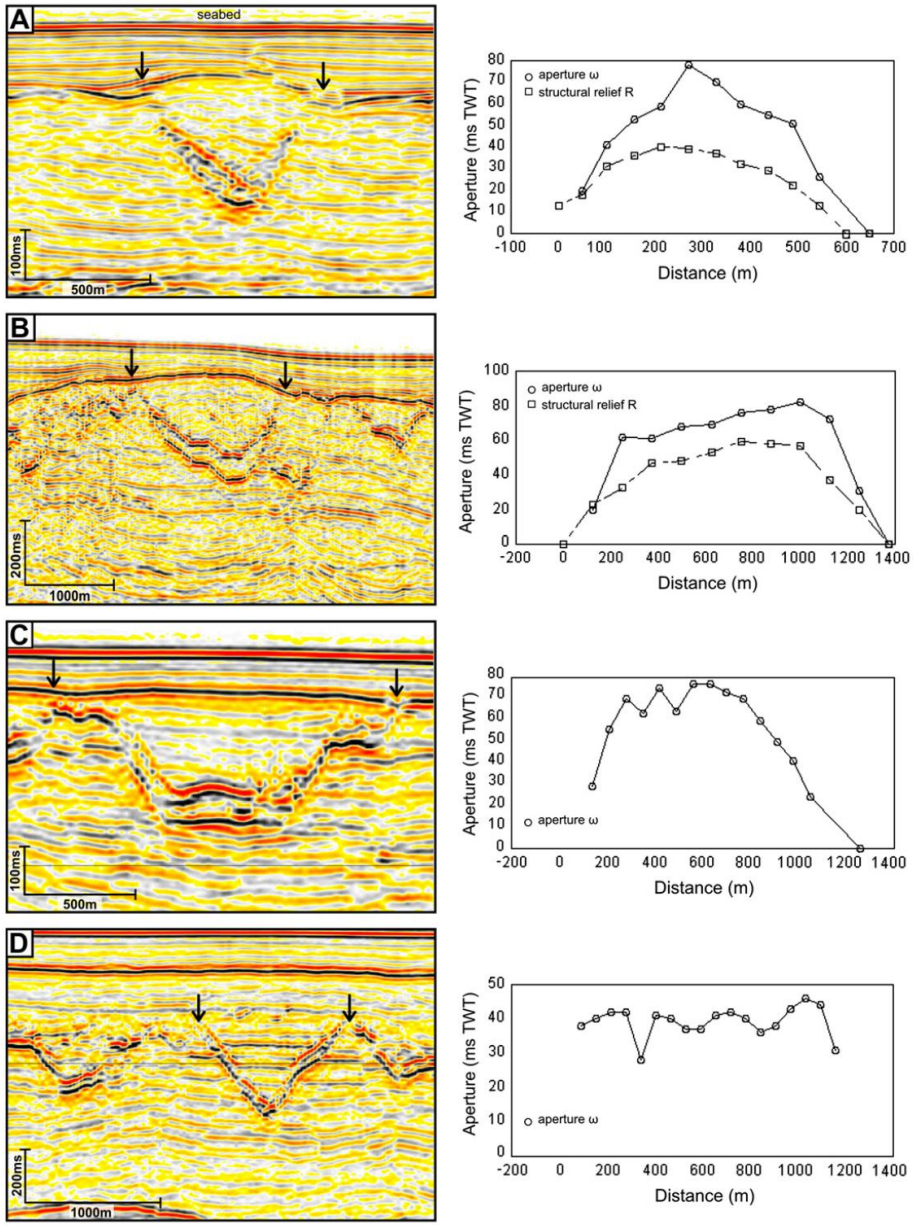

Fig. 9. Aperture (ω) versus distance plots for four representative intrusions from the Faeroe–Shetland Basin, along with measurements of structural relief on accompanying forced folds, where preserved. Aperture values are in milliseconds TWT (1 ms approximately equal to 1 m), arrows on profiles denote start and end points of graphed data. (A) A simple apical cone, with clear wedge-like tapering towards the tips. (B) A stepped flat-based bowl (see also Fig. 10), with a close match between ω and structural relief, R. (C) A classical flat-based bowl, but a probably eroded forced fold. (D) A sharp apical cone, with a tabular distribution of ω, and a flat-topped hydraulic elevation of the overburden, seen in the relative elevations of a pair of prominent reflections inside and outside the structure. Data courtesy of Exxon-Mobil Ltd.

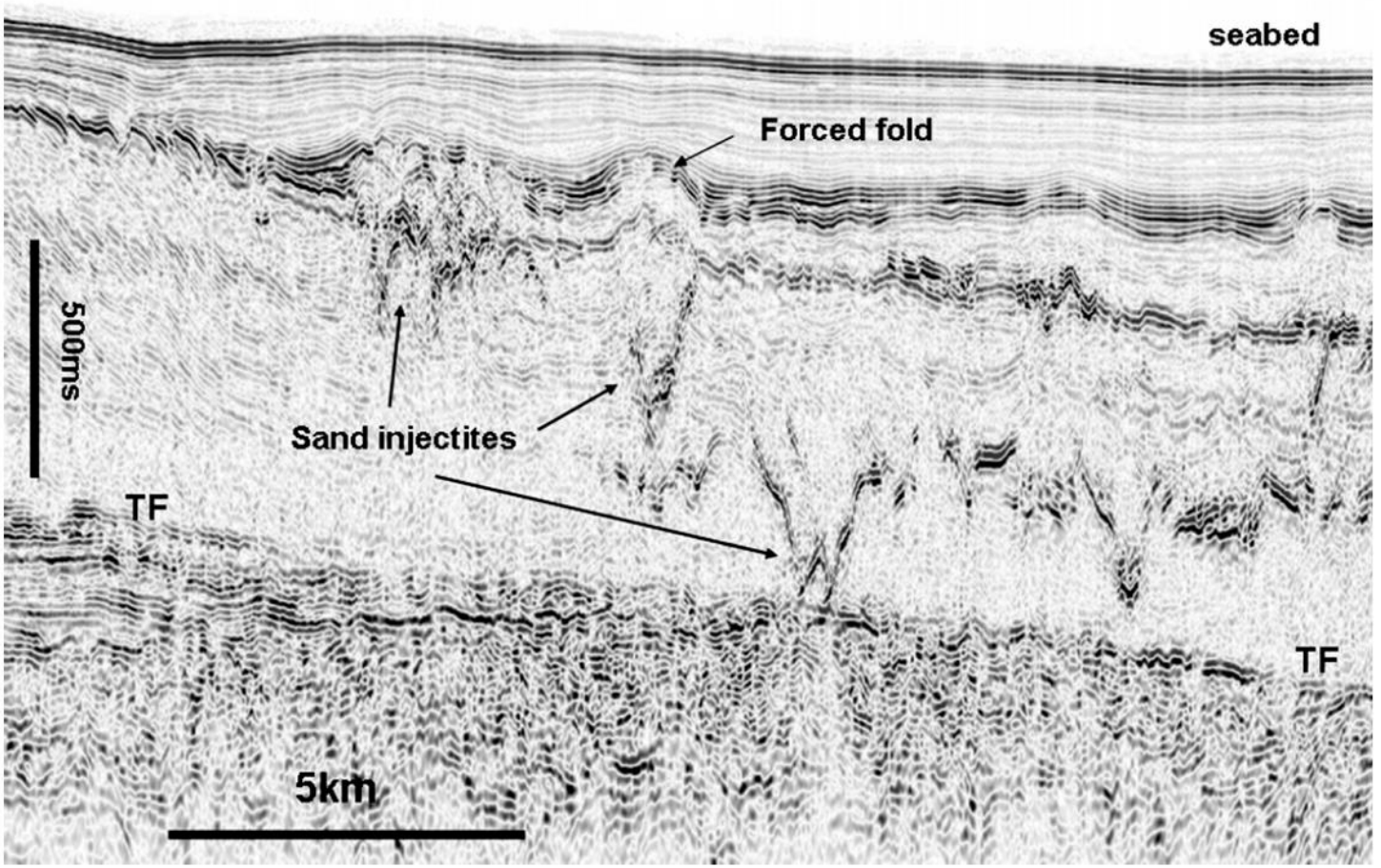

Fig. 4. Seismic profile across the Cuillin Fan in the Faeroe–Shetland Basin, showing discordant amplitude anomalies interpreted as sand injectites emanating from the top of the submarine fan sandstone (TF), and intruded upwards for over 700 m through polygonally faulted Eocene claystones (faults seen clearly on left hand side of the profile). Forced folds at the Miocene unconformity are evidence of the timing of the intrusion event. Data courtesy of Exxon-Mobil Ltd.

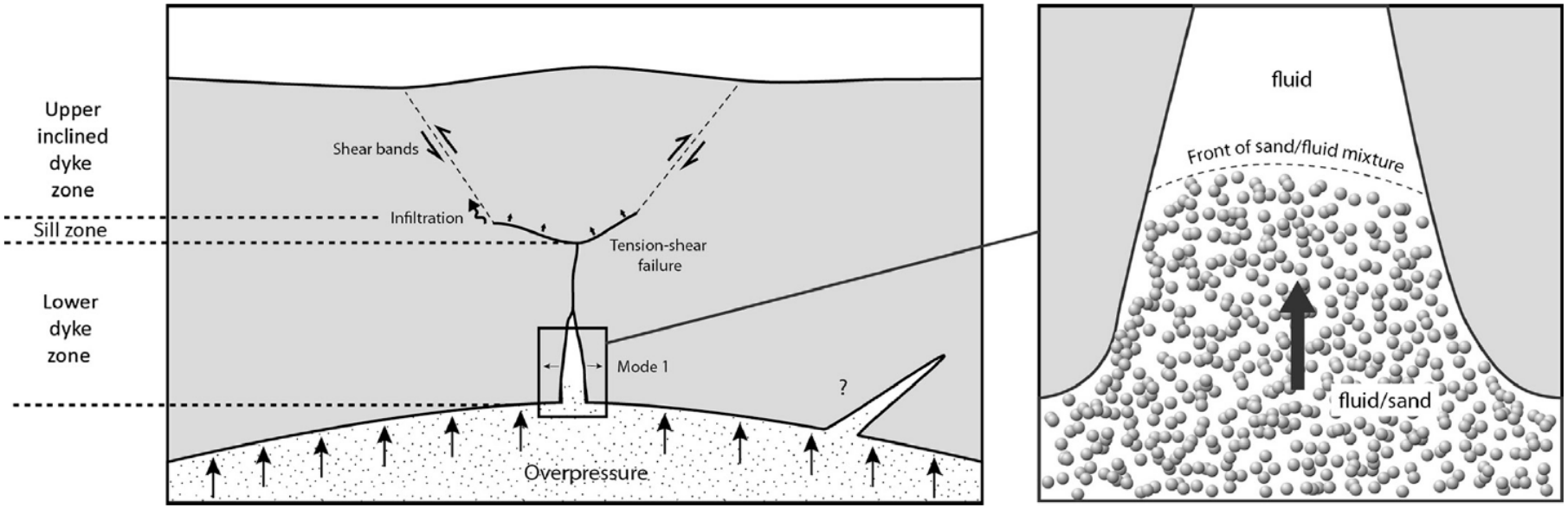

Fig. 1. Sketch showing the main physical processes relevant to sandstone intrusion. On the left, an increase of reservoir pore fluid pressure leads to a vertical hydraulic fracture opening in Mode I, at a critical depth; it splits into two branches opened in mixed mode before using shear bands as a conduit for fluid. This tripartite architecture can be compared with field observations (Vigorito and Hurst (2010). Wings-like intrusions are inclined intrusions departing over the periphery of a parent sand body. The emplacement mechanisms of such structures are poorly constrained. On the right, sand fluid mixture is fluidised and injected into fractures.

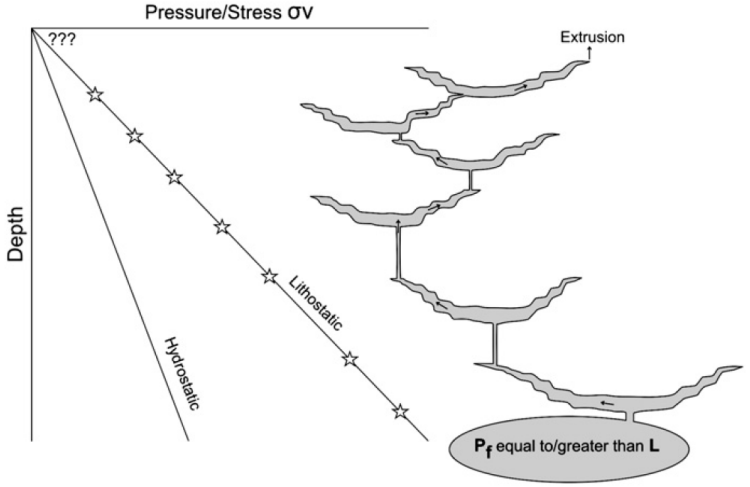

Fig. 14. Schematic pressure-depth plot for the intrusion complex in the Faeroe–Shetland Basin, during peak conditions of flow once the fracture network had formed. The pore fluid pressure in the parent body is inferred to have been equal to or greater than lithostatic because sills are observed to emanate from the top of this unit (Shoulders et al., 2007). The star symbols represent the minimum fluid pressures required in the overlying interconnected conical intrusions to keep open a continuous conduit and to permit flow from the parent body to the top of the intrusion complex.

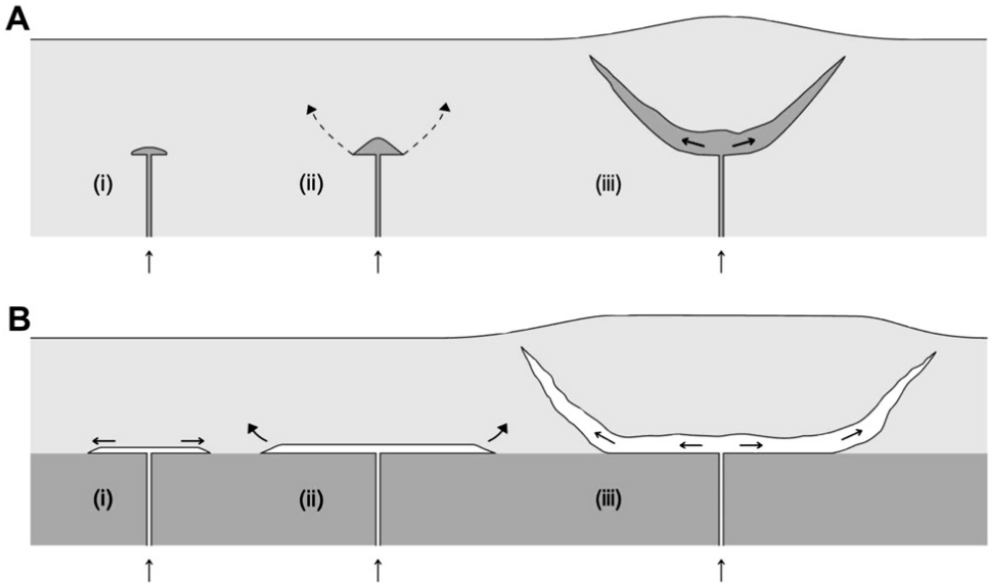

Fig. 12. Schematic model showing the propagation of apical cones (A) and flat-based bowls (B). In (A), a feeder delivers a sand flux to a seed point, where a small laccolith intrusion forms, possibly at a minor competence contrast. This local pressure focus then promotes the propagation of conical fractures in direct analogy with cone sheet formation. In (B), the competence contrast at a boundary is greater, and promotes lateral propagation and not inflation. Once the dimensions of the sill reach a critical value, the fracture interacts with the free surface, and the sill turns upwards towards the surface.

Intrusion type	Type 1	Type 2a	Type 2b	Type 3
Schematic representation				
Limb dips (°)	5.5 < X < 44	42 < X < 68	25 < X < 52	Not measured
Height (m)	77 < X < 215	168 < X < 259	140 < X < 238	Not measured
Top diameter (m)	534 < X < 1139	345 < X < 790	399 < X < 849	Not measured
Associated polygonal fault strikes		N128°E<X<N169°E	N118°E<X<N174°E	N34°E<X<N69°E

Fig. 9. Table showing schematic representation of the different intrusions types and summarizing main geometrical information. Ranges of polygonal fault strikes interacting with sandstone intrusions is also given.

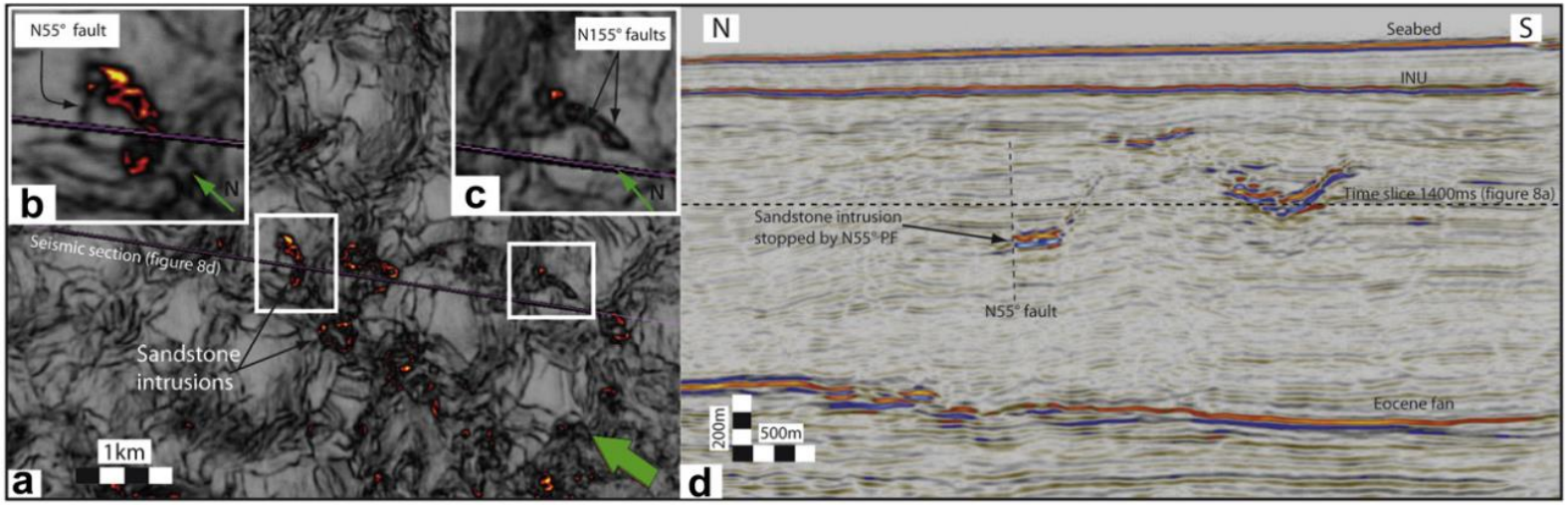

Fig. 8. a) Variance time slice at 1400 ms across orphan half conical sandstone intrusion, red and yellow colours highlight the occurrence of sandstone intrusions. White squares correspond to Figures b and c, black straight line shows the position of Figure d. B, displays a half conical sandstone intrusion, note that this intrusion is stopped by a N055°E fault visible on Figure d. C, underlines an intrusion gently intruded into N155°E faults. C is not represented on d) but may correspond to Fig. 4c. D, is an amplitude cross section with the position of 1400 ms time slice (Fig. 8a). (For interpretation of the references to colour in this figure legend, the reader is referred to the web version of this article.)

Geology, May 2012; v. 40; no. 5; p. 467–470; doi:10.1130/G33117.1; 4 figures; Data Repository item 2012133.

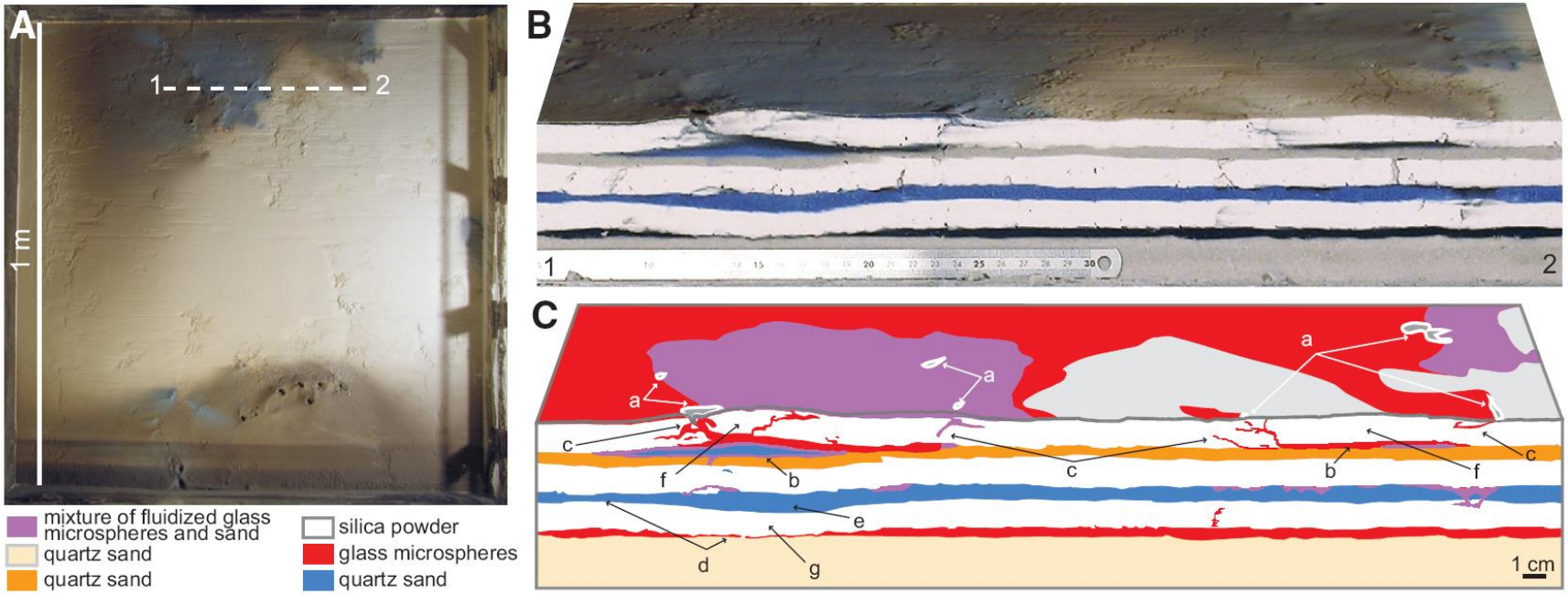

Figure 4. Experimental model of formation of sand injectites (after Rodrigues et al., 2009). Duration of experiment was 10 min. Images are for final state. A: Photograph of horizontal surface shows material (blue and black) that erupted through vents, when fluid pressure exceeded weight of overburden. Dashed line (1–2) is trace of cross section. B: Oblique photograph shows cross section together with top surface of model (for section line, see A). C: Line drawing interpretation of oblique view in B. Model was 1 m long and 1 m wide (A) and consisted of 7 layers (B, C). From top to bottom, layers 1, 3, and 5 were of silica powder (1.5 cm thick, white in B and C); layers 2 and 4 were of quartz sand (0.5 cm thick, gray and blue in B, orange and blue in C); layer 6 was of glass microspheres (0.5 cm thick, black in B, red in C); and layer 7 was of quartz sand (2 cm thick, gray in B, light yellow in C). Glass microspheres and blue sand erupted simultaneously through vents (a) and filled fractures within layer of silica powder and at interface between upper silica powder and white sand (b), forming sills and laccoliths. Wings at terminations of some laccoliths and sills (c) fed vents at surface. Beneath these vents, corresponding source layers thinned (d), as result of depletion, while others became thicker (e). In roofs of laccoliths, uppermost layer of silica powder formed domes (f) as result of bending. In some areas, where layer of glass microspheres lost volume, overlying layer of silica powder bent downward (g).

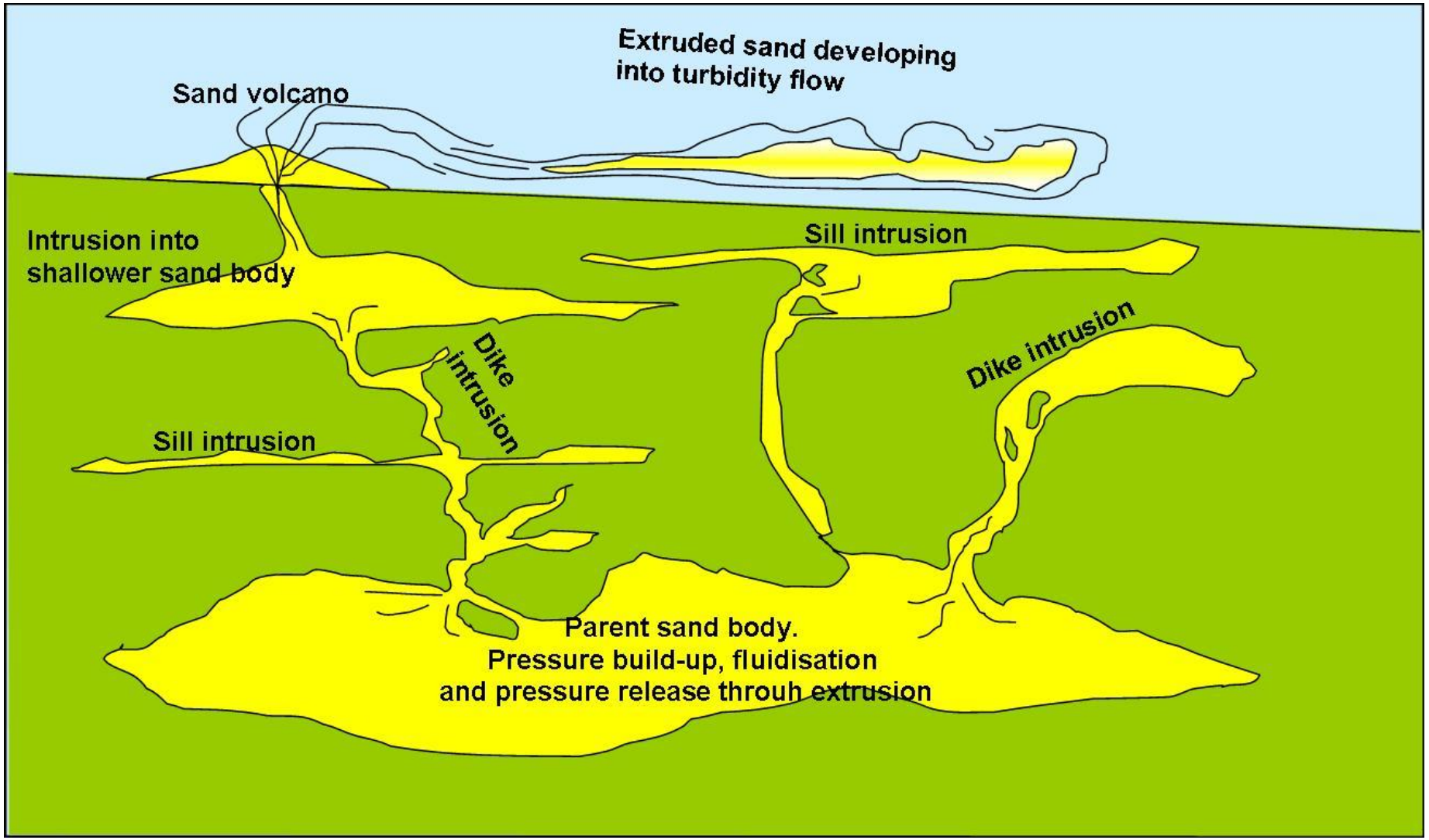

Sketch showing various sand intrusion to extrusion types.

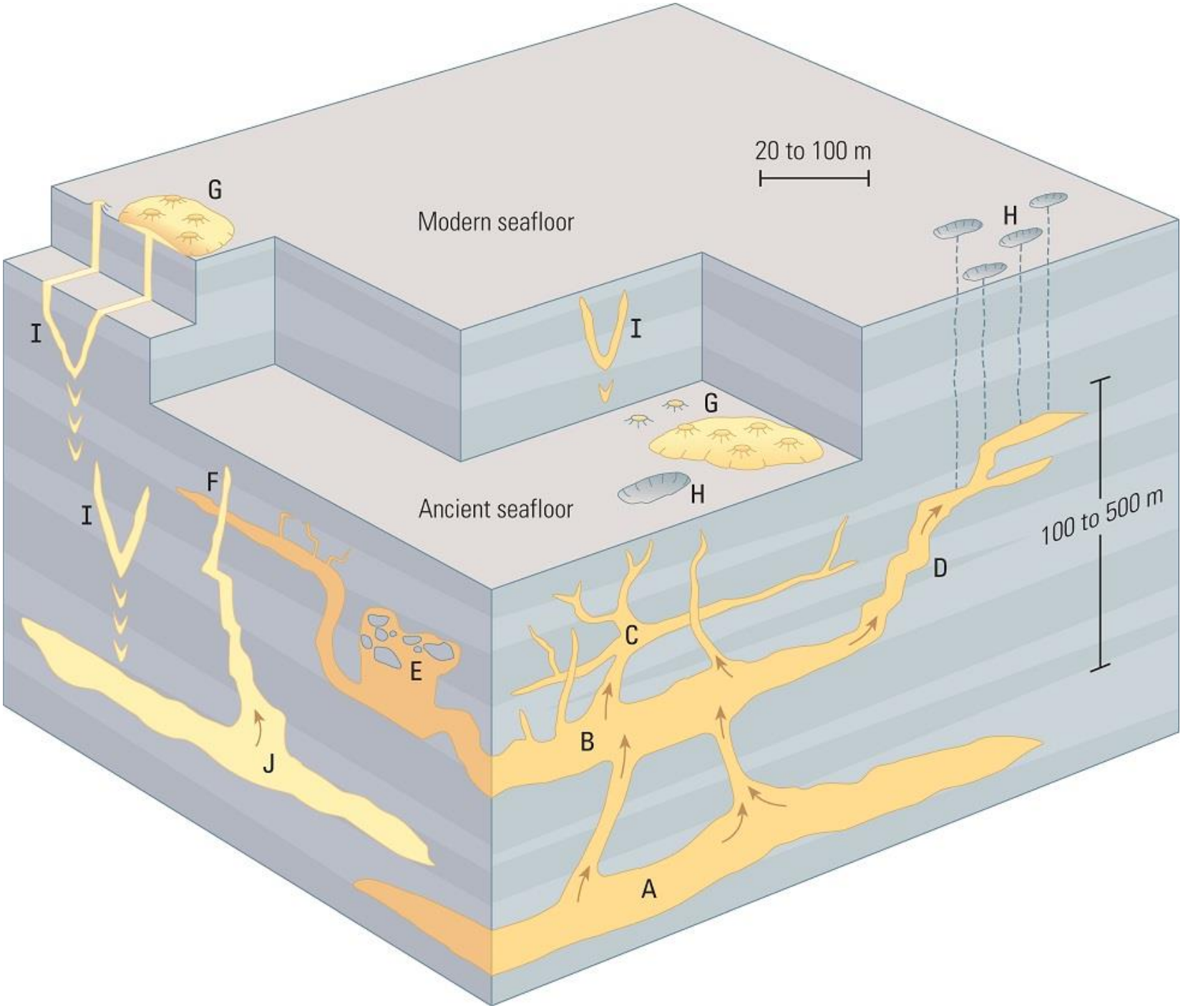
20 to 100 m
Modern seafloor
Ancient seafloor
100 to 500 m
A
B
C
D
E
F
G
H
I
J

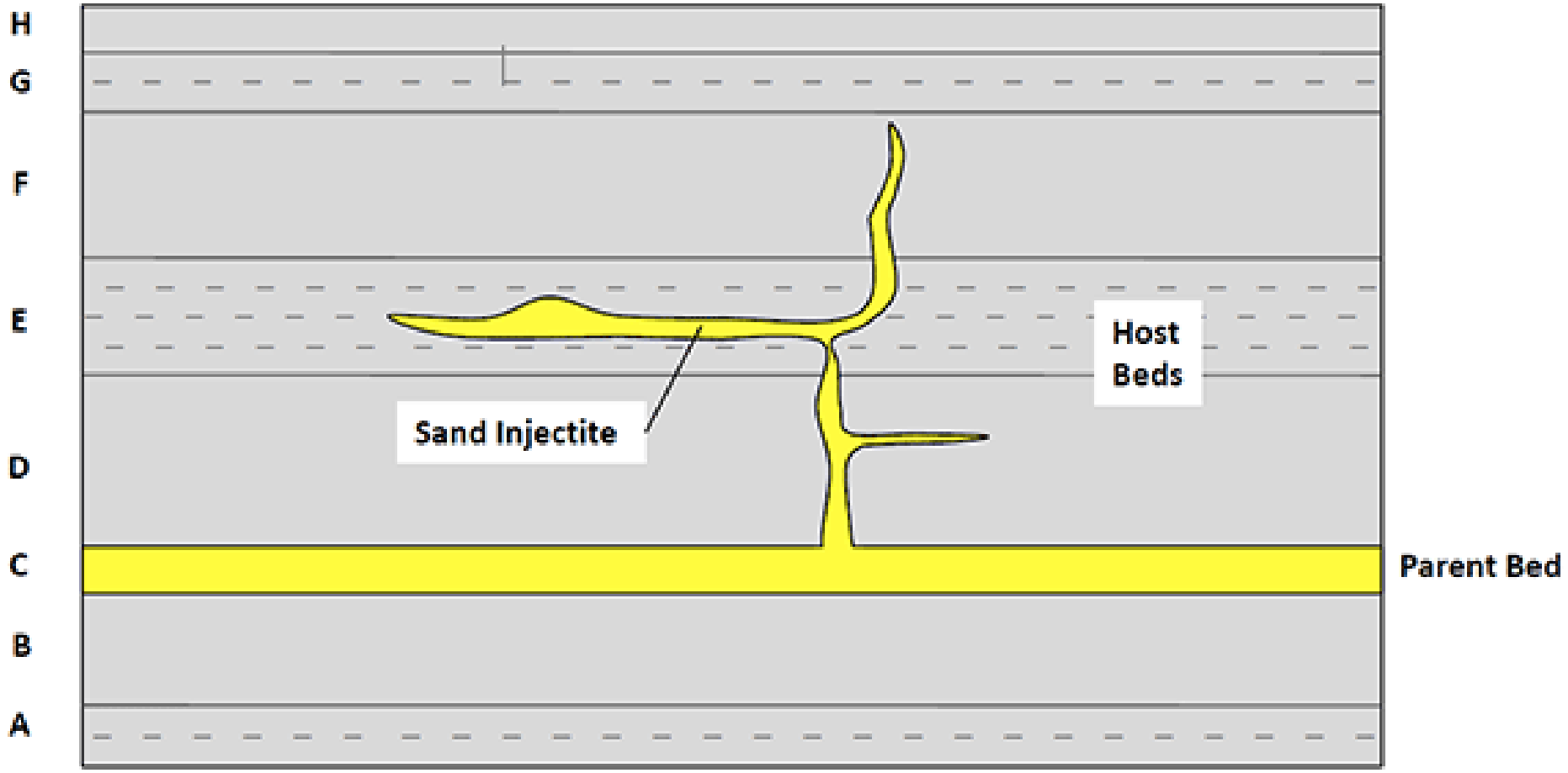
H
G
F
E
D
C
B
A
Host Beds
Sand Injectite
Parent Bed

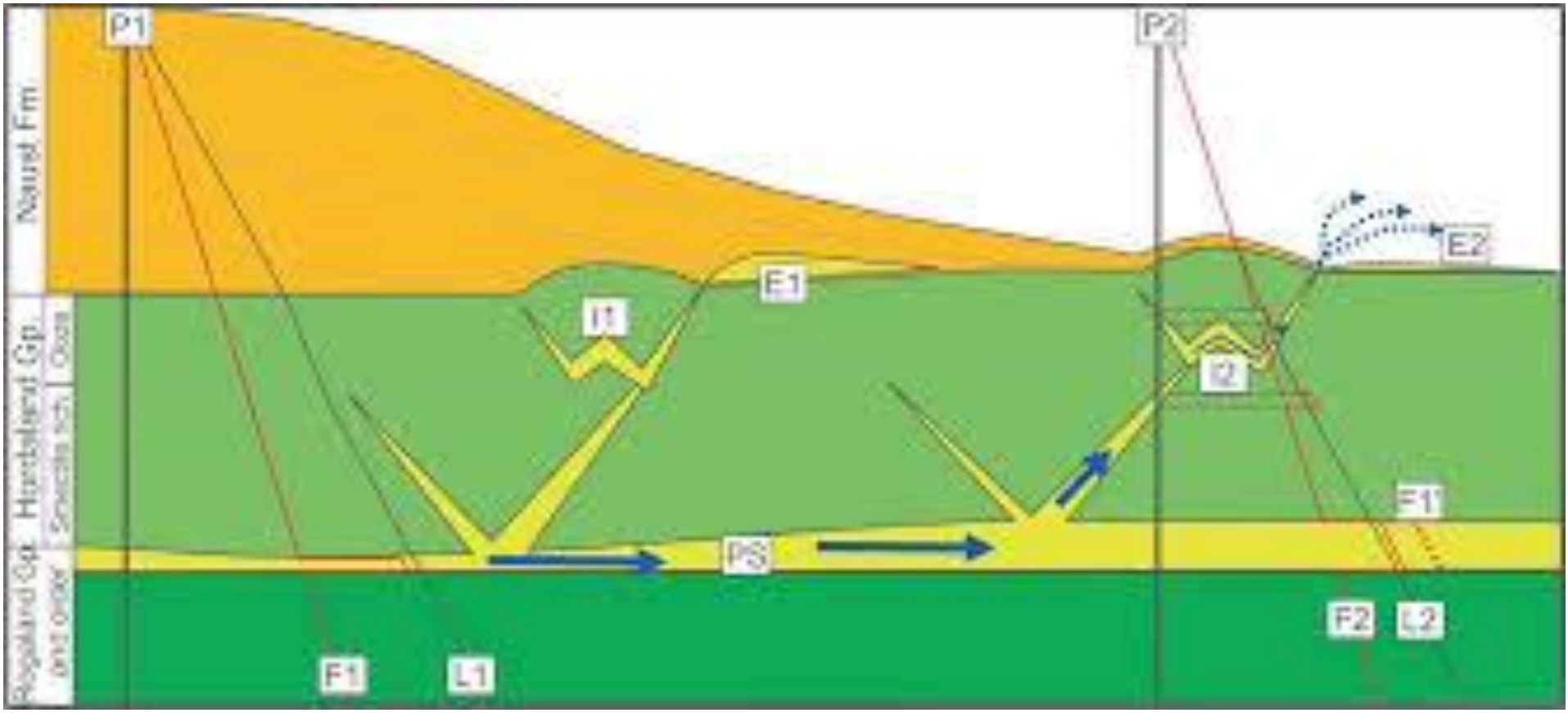
Nauvel Fm
Hordaland Gp.
Rogaland Gp.
Øvre
Skade Fm
Ekofisk Fm
Tor Fm
P1
P2
E1
E2
I1
I2
PS
F1
L1
F2
L2

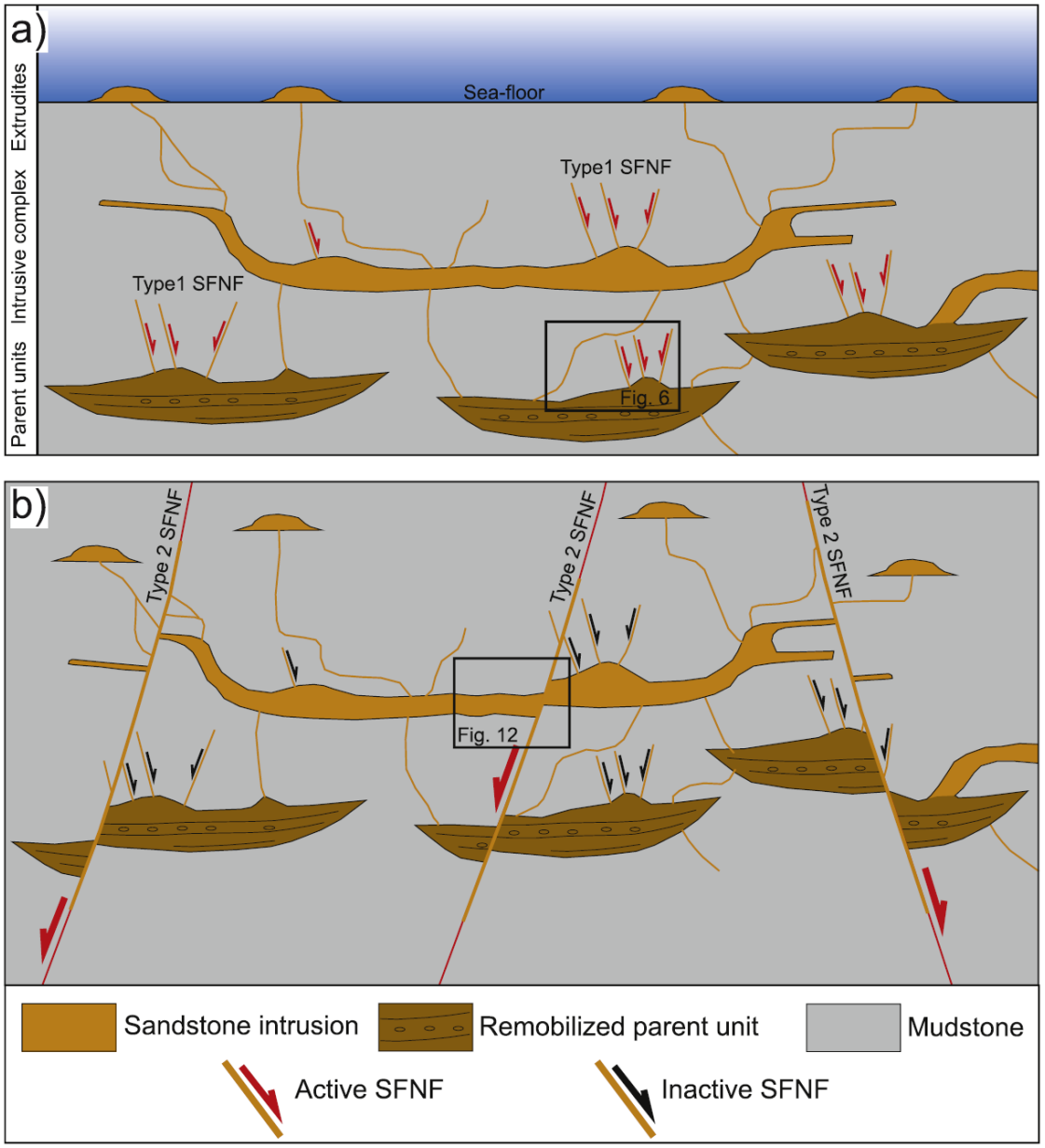

Fig. 11. Simplified model of the cross-cutting relationships between Type 1 SFNF and Type 2 SFNF as observed in the PGIC, TGIC and SCIC. a) Emplacement of a sand injection complex. The different architectural elements are organized as proposed by Vigorito et al. (2008). Type 1 SFNF form concomitantly with this event and the age of the faults, as well as that of the entire complex, is obtained by dating the mudstones at the base of the extrudites. b) The emplacement of Type 2 SFNF occurs during a faulting event post-dating the emplacement of the main complex. The age of these faults can be determined using standard methods (model is not to scale).

Песчаные интрузивные тела на суше

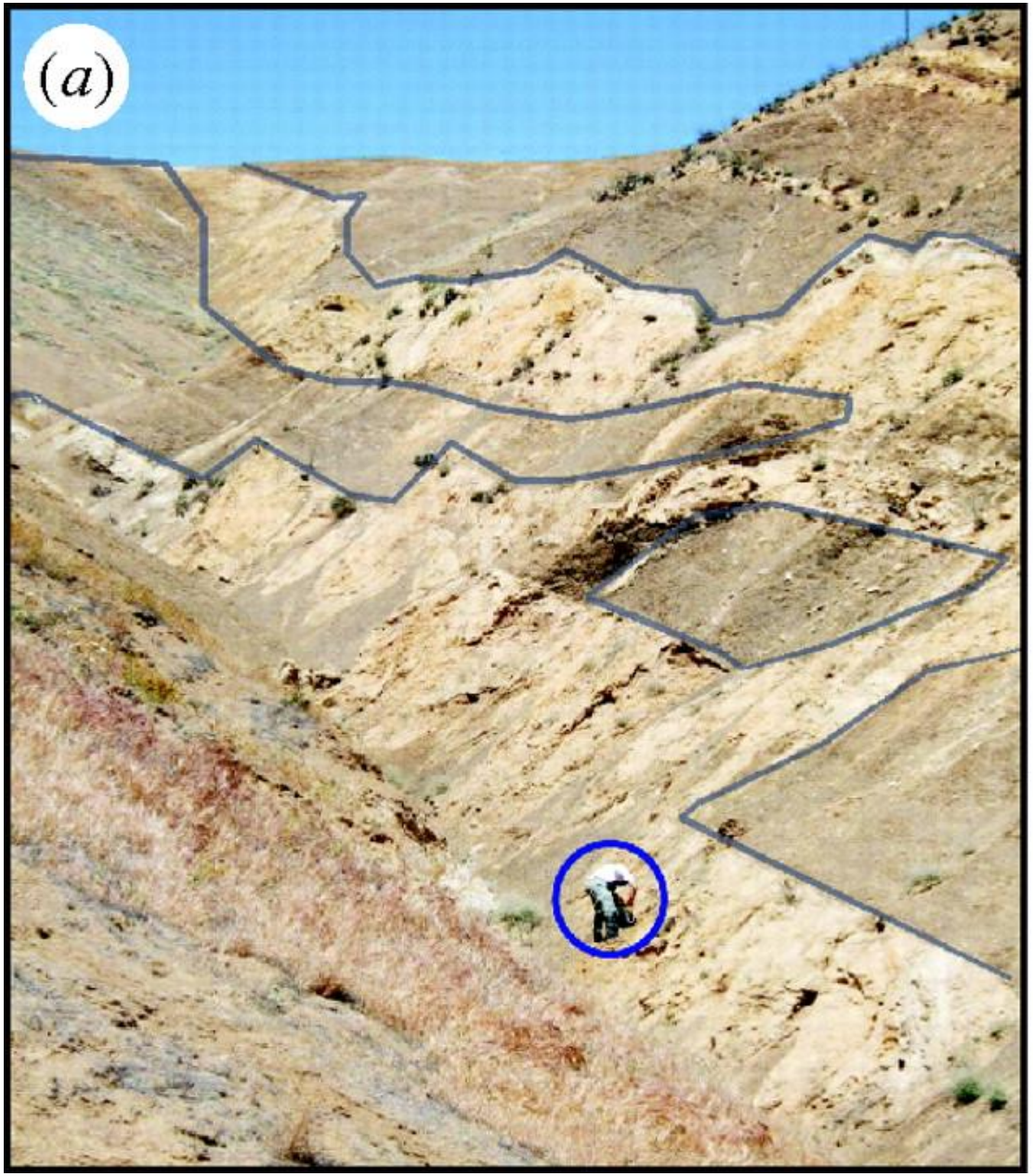

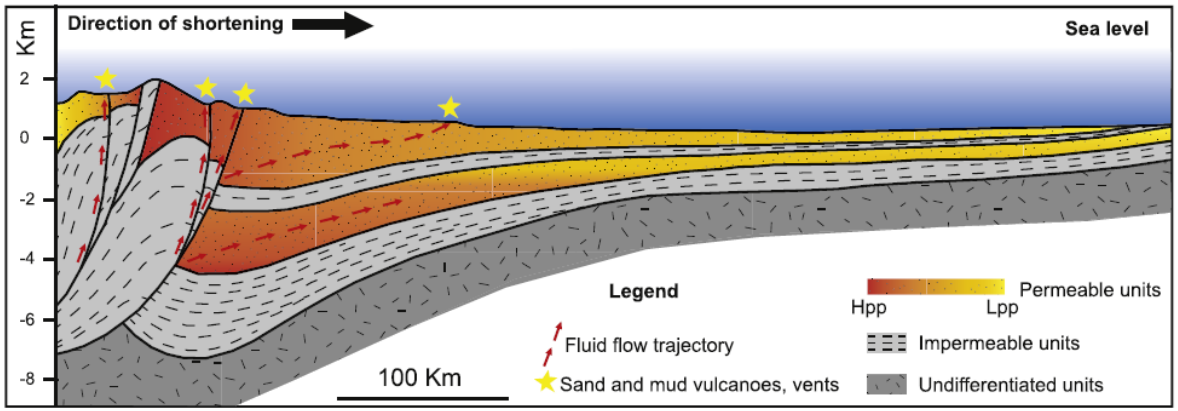

Fig. 1. Simplified model showing the main fluid migration pathways in an orogenic belt (after Oliver, 1986). A huge amount of water is generated and then expelled because of contractional deformation in thrust and fold belts. Hpp: high pore-pressure; Lpp: low pore-pressure.

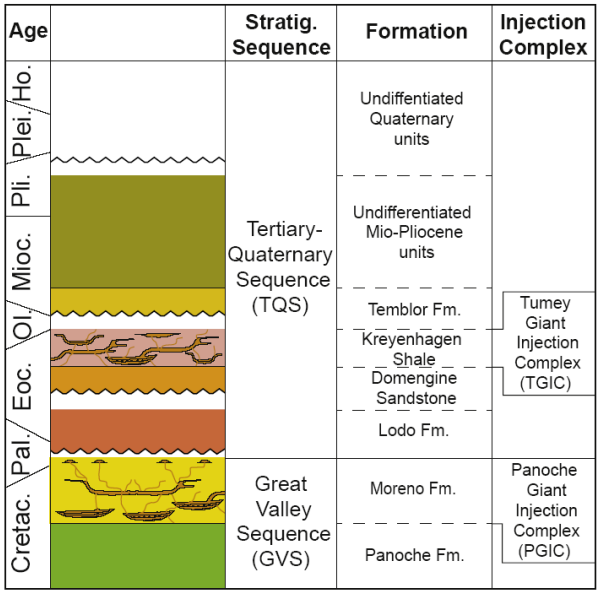

Fig. 3. Stratigraphic column showing the geological units cropping out in the Panoche and Tumey hills (modified from Bartow, 1996). The stratigraphic position of the giant sand injection complexes is marked. GVS-Great Valley Sequence; TQS-Tertiary to Quaternary Sequence; PGIC-Panoche Giant Injection Complex; TGIC-Tumey Giant Injection Complex.

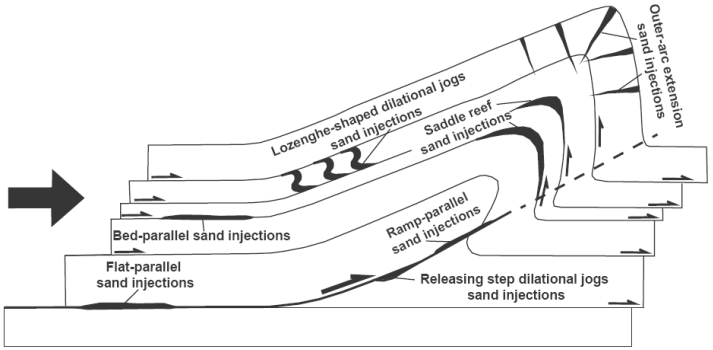

Fig. 4. Simplified model showing the distribution of fluidized sand in a thrust (modified from Erslev and Mayborn, 1997). Intrusions preferentially occur along the thrust surface, and also in dilatant cavities in the hangingwall and footwall of the thrust.

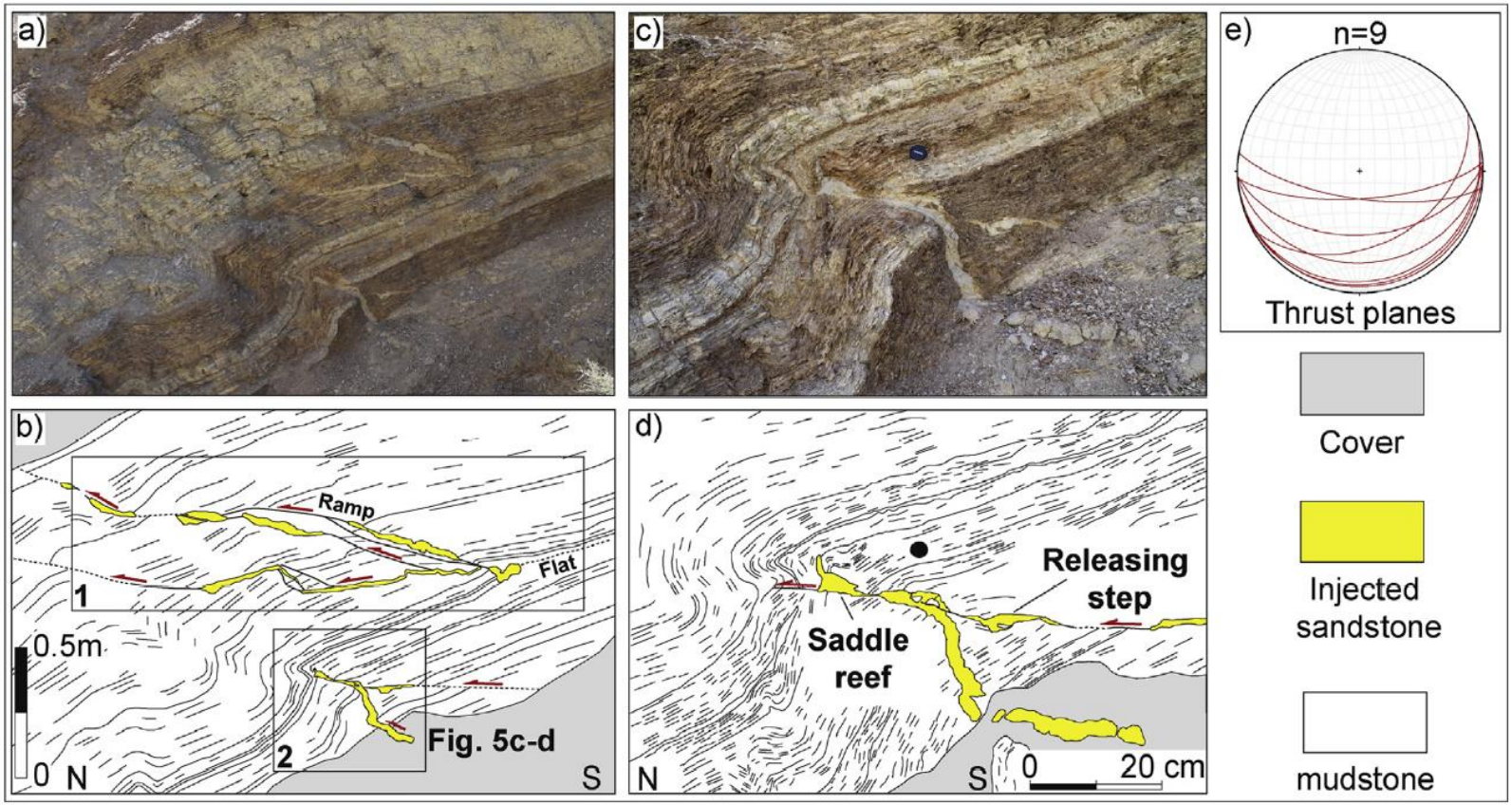

Fig. 5. a) Photograph and b) associated line drawing of outcrop MR1 (36°30.709′N 120° 32.989′W) showing two stacked N-verging sandstone-filled thrusts (in boxes). c) Photograph and d) associated line drawing showing detail of the blind sandstone-filled thrust from 5a. Note that the offset across the thrust progressively decreases toward the tip of the intrusion. e) Lower hemisphere equal area stereographic projection showing the orientation of the thrust planes (great circles).

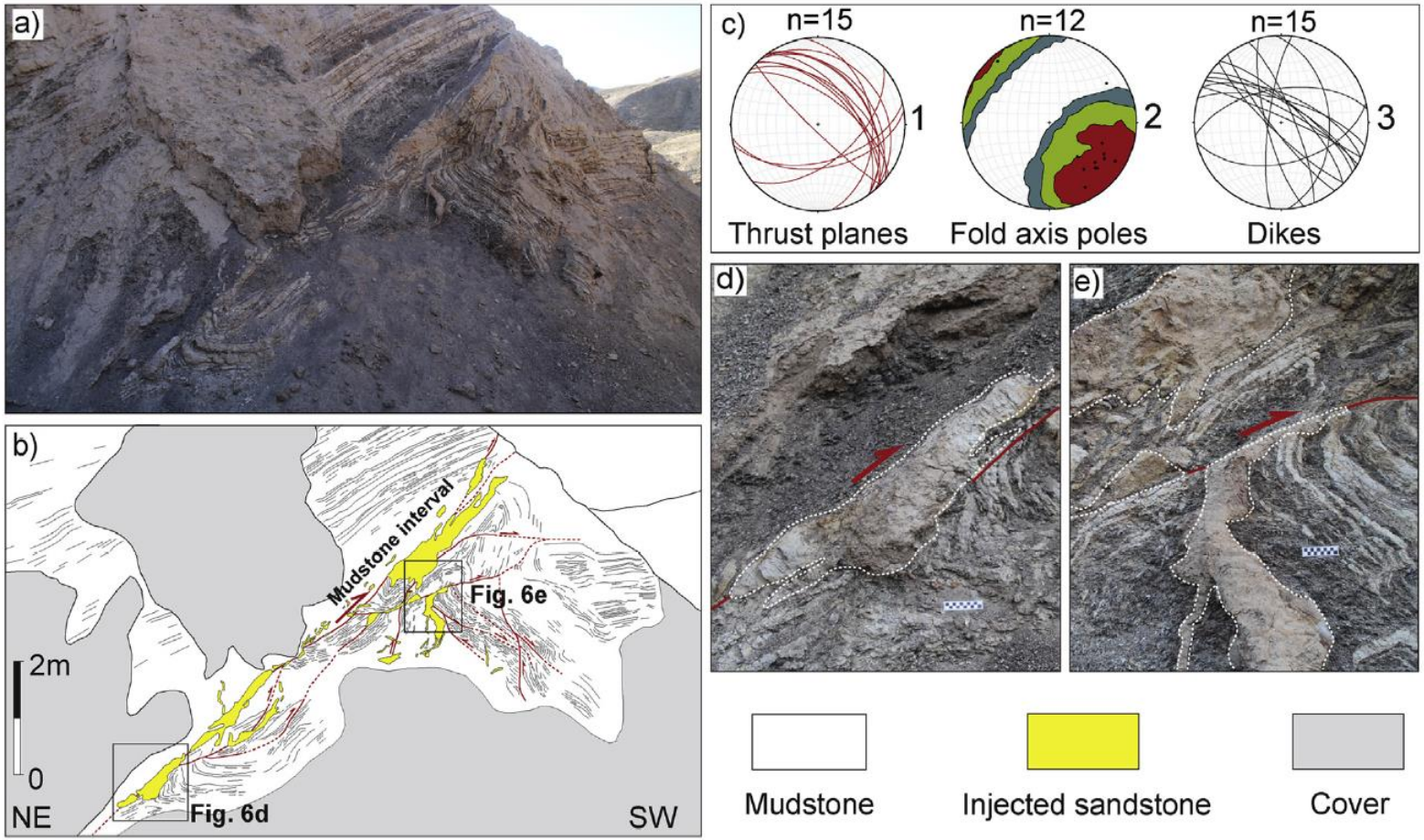

Fig. 6. a) Photograph and b) associated line drawing of outcrop at Tumey Gulch (TG1) (36° 31.215′N 120° 38.407′W) showing a SW-verging thrust filled by sandstone intrusions. c) Equal area lower hemisphere stereographic projections showing two different thrust trends visible on plot 1. Contoured fold hinges are shown in plot 2, while dike orientations (plot 3) display a similar orientation to the trend of the thrusts. d) and e) Details of the sandstone-filled thrust (see Fig. 6b), note that the sandstone intrusion initially follows bedding planes and then turns abruptly to intrude along the thrust surface.

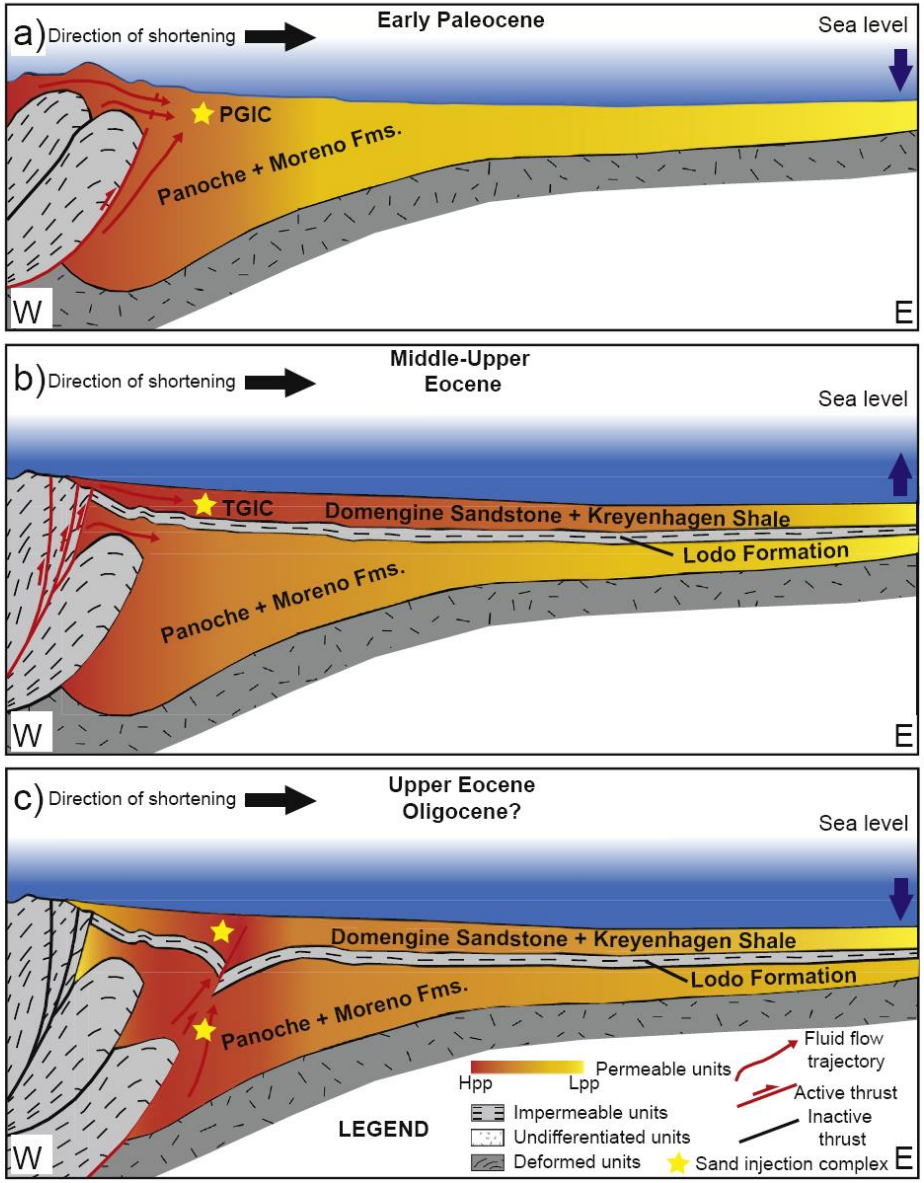

Fig. 19. Diagrams showing the proposed evolutionary model for the emplacement of sandstone intrusions in the study area of the San Joaquin Valley during Early-Middle Cenozoic (thickness of the different units not to scale). a) Emplacement of PGIC during the Danian in the upper portion of the Moreno Formation at the beginning of the Laramide orogeny. b) Emplacement of the TGIC during Middle-Upper Eocene. c) Emplacement of sand-filled thrusts during Late Eocene-Oligocene when the study area was directly affected by contractional tectonics. Fluid migration occurred along tectonic discontinuities leading to the emplacement of the sandstone-filled thrusts. Hpp: high pore-pressure; Lpp: low pore-pressure.